

Authors' Note: This is a preprint version of the article currently under review. We welcome constructive feedback and comments to further enhance the quality and clarity of this work. If you have any suggestions, insights, or critiques, please feel free to contact the corresponding author, Mohammad Asif Habibi[✉], at [mohammad_asif.habibi@dfki.de]. We sincerely appreciate all feedback, whether minor, critical, or substantial.

Disclaimer: This article has been submitted to the IEEE for possible publication. Copyright may be transferred without notice, after which this version may no longer be accessible.

Copyright: © 2026 IEEE. Personal use of this material is permitted. If the article gets accepted, permission from IEEE must be obtained for all other uses in any current or future media, including reprinting/republishing this material for advertising or promotional purposes, creating new collective works, for resale or redistribution to servers or lists, or reuse of any copyrighted component of this work in other works.

SliceMapper: Intelligent Mapping of O-CU and O-DU onto O-Cloud Sites in 6G O-RAN

Mohammad Asif Habibi[✉], Xavier Costa-Pérez[✉] (*Senior Member, IEEE*), and Hans D. Schotten[✉] (*Member, IEEE*)

Abstract—In this paper, we propose an rApp, named **SliceMapper**, to optimize the mapping process of the open centralized unit (O-CU) and open distributed unit (O-DU) of an open radio access network (O-RAN) slice subnet onto the underlying open cloud (O-Cloud) sites in sixth-generation (6G) O-RAN. To accomplish this, we first design a system model for **SliceMapper** and introduce its mathematical framework. Next, we formulate the mapping process addressed by **SliceMapper** as a sequential decision-making optimization problem. To solve this problem, we implement both on-policy and off-policy variants of the Q -learning algorithm, employing tabular representation as well as function approximation methods for each variant. To evaluate the effectiveness of these approaches, we conduct a series of simulations under various scenarios. We proceed further by performing a comparative analysis of all four variants. The results demonstrate that the on-policy function approximation method outperforms the alternative approaches in terms of stability and lower standard deviation across all random seeds. However, the on-policy and off-policy tabular representation methods achieve higher average rewards, with values of 5.42 and 5.12, respectively. Finally, we conclude the paper and introduce several directions for future research.

Index Terms—5G, 6G, Non-RT RIC, O-Cloud Sites, O-CU, O-DU, O-RAN, O-RAN Slicing, Off-policy, On-policy, Q -Learning, rApps, Reinforcement Learning, SMO, **SliceMapper**

I. INTRODUCTORY REMARKS

THE *mapping* of virtual network functions (VNFs) onto the underlying physical infrastructure presents a complex *optimization* problem [1]. This problem has been extensively studied over the last decade in the context of cloud computing [2]. However, with the extension of *virtualization* and *cloudification* to the edge of cellular networks, combined with the unique characteristics of wireless communication *channels* and the diverse *requirements* of end-users and vertical industries, the VNF mapping problem has become even more intricate [3]. Furthermore, the recent introduction of *open* interfaces and multi-vendor *interoperability* in fifth-generation (5G) and sixth-generation (6G) open radio access

network (O-RAN) has further amplified the complexity of VNF mapping [4]. Therefore, it is essential to reconsider traditional solutions and re-evaluate the properties of this optimization problem in light of these *new* challenges.

In O-RAN, the traditional *monolithic* base station, namely open next generation node B (O-gNB), is decomposed into open centralized unit (O-CU), open distributed unit (O-DU), and open radio unit (O-RU), which communicate over standardized open interfaces [5]. The O-CU and O-DU (as VNFs) can be deployed on heterogeneous open-cloud (O-Cloud) sites and the O-RU on cellular network sites. This architectural shift enables multi-vendor interoperability, flexible deployment, and *network slicing*, but it also significantly increases the complexity of virtual and physical resource management [3]. In particular, the mapping of O-CU and O-DU onto available virtual machines (VMs) in O-Cloud sites must account for diverse computational and storage requirements, stringent performance constraints, and dynamic network conditions. Hence, traditional static or rule-based mapping *strategies* become insufficient to efficiently handle the scale and variability of O-RAN deployments in beyond 5G and 6G [3].

The challenge becomes even more intensified in the context of O-RAN slicing, where multiple slice subnets with heterogeneous service requirements coexist on a shared wireless infrastructure [3]. Each slice subnet may impose different latency, throughput, and reliability constraints, requiring intelligent and adaptive mapping of VNFs to avoid resource underutilization or congestion [3]. Moreover, the O-RAN service management and orchestration (SMO) framework introduces the concept of rApps operating in the non-real-time RAN intelligent controller (Non-RT RIC) [6], enabling data-driven and policy-based optimization over long time scales. While this creates an opportunity to leverage artificial intelligence (AI)/machine learning (ML) for O-RAN optimization, it also raises fundamental questions regarding how learning-based approaches should be designed, trained, deployed, and evaluated for complex VNF mappings in large discrete action spaces [7].

This manuscript was received on DD MM 2026, revised on DD MM 2026, and accepted on DD MM 2026. It was published on DD MM 2026, and the current version was last updated on DD MM 2026.

Mohammad Asif Habibi[✉] and Hans D. Schotten[✉] are with the Intelligent Networks (IN) Research Department, German Research Center for Artificial Intelligence (DFKI), 67663 Kaiserslautern, Germany. Xavier Costa-Pérez[✉] is with the 6G Networks R&D Department, NEC Laboratories Europe, 69115 Heidelberg, Germany. He is also associated with the Department of AI-Driven Systems of the i2CAT Research Center and the Department of Engineering Sciences of the Catalan Institution for Research and Advanced Studies (ICREA), 08034 Barcelona, Spain. Hans D. Schotten[✉] is also affiliated with the Division of Wireless Communications and Radio Navigation (WiCoN), Department of Electrical and Computer Engineering (EIT), University of Kaiserslautern (RPTU), 67663 Kaiserslautern, Germany. The corresponding author is Mohammad Asif Habibi[✉] (mohammad_asif.habibi@dfki.de).

A. Prior Works

To this end, several methodologies have been proposed to study VNF mapping in both cloud/data center and wireless network environments, including approaches based on AI/ML techniques. A comprehensive comparison of representative state-of-the-art works is provided in Appendix A. Notably, existing studies generally model each VNF as a monolithic entity and investigate its mapping onto the available underlying physical machines (PMs). Furthermore, most works primarily address VM-to-PM placement problems. Consequently, they typically virtualize the compute and storage resources of PMs

first and subsequently allocate these virtualized resources to VNFs in the form of VMs or containers.

B. Major Research Challenges

However, **the monolithic treatment of VNFs during the mapping process**, together with **the reliance on conventional optimization approaches**, particularly in the context of O-RAN slicing, introduces several additional limitations. First, each VNF within an O-RAN slice **typically comprises multiple micro-functionalities** [3], each of which may require different amounts of virtual compute and storage resources to execute a given set of tasks. Second, **the execution requirements of these micro-functionalities may vary significantly** across different slice subnets [8]. For example, a specific functionality may be disabled or require substantially more or fewer resources in one type of slice subnet compared to another. Consequently, modeling and mapping a VNF as a monolithic entity, specifically across various types of O-RAN slice subnets, **becomes increasingly inefficient and difficult to scale**. Therefore, this optimization problem warrants reexamination within the broader context of O-RAN slicing.

C. Design Goals and System Objectives

To address the aforementioned research challenges, we adopt a strategy that departs from existing methodologies and is grounded in the following novel design choices. First, **we decompose each VNF (i.e., O-CU and O-DU) of an O-RAN slice subnet into multiple micro-functionalities**. These micro-functionalities are referred to as virtual network function components (VNFCs), following the terminology defined by the European Telecommunications Standards Institute (ETSI) [3]. To the best of our knowledge, this work is the first to incorporate VNF decomposition into micro-functionalities directly within the mapping process. While this decomposition introduces additional design considerations, it also enables finer-grained control over resource allocation; its rationale and implications are discussed in Appendix B. Second, in contrast to state-of-the-art approaches that virtualize PMs and subsequently allocate them to VNFs, **we explicitly consider the virtual resource requirements of each VNFC and select an optimal VM from a candidate set onto which the considered VNFC is mapped**. Third, unlike prior works that primarily focus on VM-to-PM placement, **our study instead targets the VNFC-to-VM mapping problem**. Fourth, **we assume that the VNFC-to-VM mapping decisions are made by an rApp deployed in the Non-RT RIC and executed by the resource manager of an O-Cloud site**. This rApp is referred to as *SliceMapper*. Finally, **we formulate the VNFC-to-VM mapping task as a sequential decision-making optimization problem** with a large discrete action space, as justified in Appendix C. To address this challenge, we investigate both on-policy and off-policy variants of *Q*-learning, a branch of reinforcement learning (RL), using both tabular representations and function-approximation methods. **This results in four distinct learning approaches, which are systematically analyzed and compared under identical experimental conditions**. The primary objective of

SliceMapper is to minimize virtual resource wastage while ensuring feasible, efficient, and scalable placement decisions across the underlying O-Cloud sites.

D. Summary of Key Contributions

In line with the objectives outlined above, the main contributions of this paper are summarized as follows:

- We **design an O-RAN-compliant system model for *SliceMapper***, which is the first rApp-based framework that addresses the mapping of VNFCs of the O-CU and O-DU within an O-RAN slice subnet onto O-Cloud sites.
- We **develop and analyze four variants of *Q*-learning**, covering both on-policy and off-policy learning, implemented using tabular representations and function approximation, to solve the VNFC-to-VM mapping problem.
- We **perform an extensive simulation-based evaluation to assess and compare** the learning behavior, convergence properties, stability, and rewards of all variants.
- We **present a comparative analysis of four variants**, revealing a clear trade-off between reward optimality and learning stability and highlighting the strengths and limitations of each approach. Specifically, **the results show that the on-policy function approximation achieves superior stability**, as evidenced by a lower standard deviation across all random seeds. In contrast, the on-policy and off-policy tabular variants achieve higher average rewards, reaching values of 5.12 and 5.42, respectively.

E. The Structure of the Paper

The remainder of this article is organized as follows. Section II presents the system model for *SliceMapper*. Section III formulates the VNFC-to-VM mapping problem along with its associated constraints. Section IV introduces the proposed *Q*-learning-based solution approach to address the optimization problem. Section V evaluates different variants of the *Q*-learning algorithm using selected performance metrics and provides a comparative analysis. Finally, Section VI concludes the paper and outlines directions for future work.

II. SYSTEM MODEL FOR SLICEMAPPER

Figure 1 illustrates the composition of the proposed system model for *SliceMapper* into three distinct *layers*: the Management and Orchestration Layer, the Network Function Layer, and the Infrastructure Layer. The Management and Orchestration Layer includes the SMO framework, which manages and orchestrates O-RAN components within a control loop operating on a timescale $t \geq 1$ second(s) [3]. This layer primarily incorporates the Non-RT RIC Framework, *SliceMapper*, and other authorized rApps. The Network Function Layer delivers the functionalities of an O-gNB, comprising an O-CU, O-DU, and an O-RU, along with the internal and external logical links of the O-gNB. The Infrastructure Layer consists of O-Cloud #1, O-Cloud #2, and the cellular network infrastructure. These sites host the O-CU, O-DU, and O-RU, respectively. Each O-Cloud site comprises of a set of VMs that are *abstracted* from the underlying PMs by the

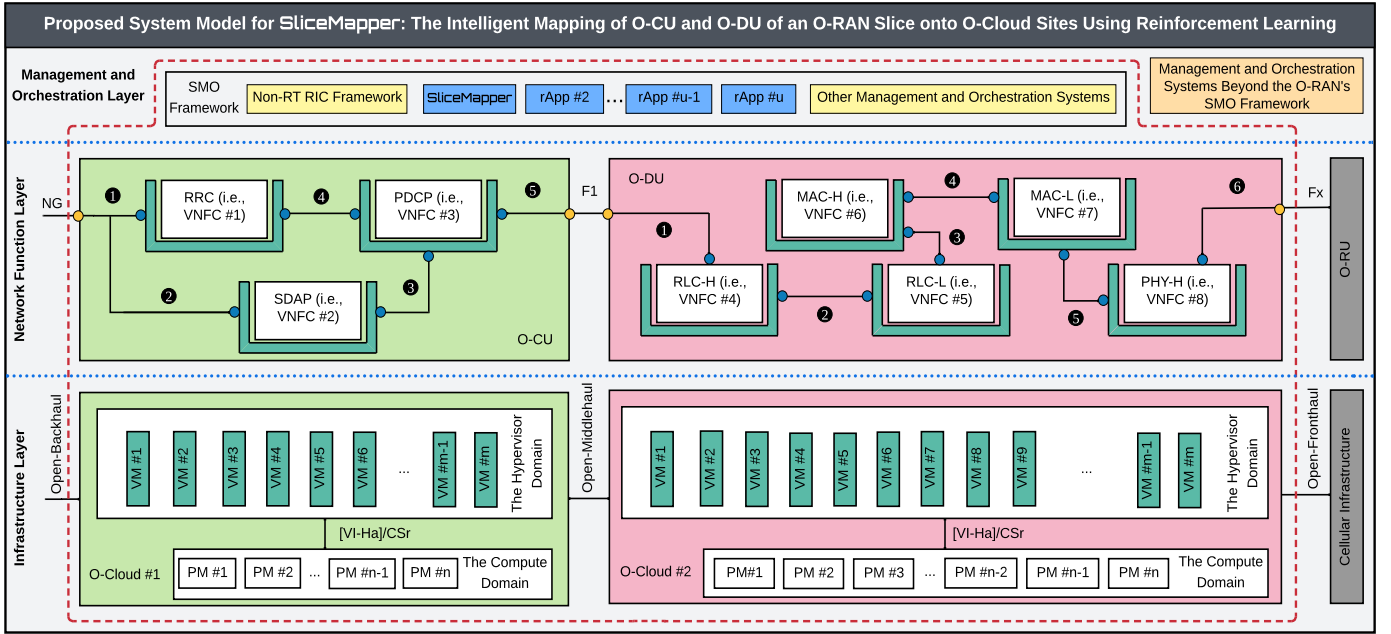


Figure 1. Proposed system model for mapping the VNFCs of the O-CU and O-DU of an O-RAN slice onto the underlying O-Cloud sites. Note that only the VNFCs of an O-gNB and their corresponding virtual resources within the O-Cloud sites, illustrated in the red-dashed box, are within the scope of this article.

Hypervisor Domain. Each VM consists of virtual compute and storage resources and hosts the VNFCs of the O-CU and O-DU within an O-RAN slice subnet. In the following subsections, we present O-RAN-compliant mathematical frameworks for the three layers of the proposed system model. Key notations related to the system model are summarized in Table I.

A. Modeling the Network Function Layer

Let $\mathcal{F} = \{f_1, f_2, \dots, f_{h-1}, f_h\}$ be a set of h physical and virtual functions of an O-RAN slice subnet, where the index $h \in \mathbb{N}$. These functions are processed sequentially by the O-CU, O-DU, and O-RU in both upstream and downstream directions [3]. We let $\mathcal{C} = \{f_1, f_2, f_3\} \subset \mathcal{F}$ be a subset of VNFCs assigned to the O-CU. In turn, let $\mathcal{D} = \{f_4, f_5, f_6, f_7, f_8\} \subset \mathcal{F}$ be a subset of VNFCs assigned to the O-DU. The subset $\mathcal{R} \subset \mathcal{F}$ constitutes the remaining functions of \mathcal{F} . These functions are the physical functions processed in the O-RU. It is worth noting that \mathcal{C} , \mathcal{D} , and \mathcal{R} are pairwise disjoint sets, meaning their intersection is an empty set (\emptyset). Additionally, the details of \mathcal{R} are beyond the scope of this paper.

Functions f_1, f_2 , and f_3 correspond to the radio resource control (RRC), packet data convergence protocol (PDCP), and service data adaptation protocol (SDAP), respectively. Functions f_4, f_5, f_6, f_7 , and f_8 represent the radio link control (RLC)-High, RLC-Low, medium access control (MAC)-High, MAC-Low, and physical (PHY)-High, respectively. Each VNFC is assumed to be hosted by a *single* VM (or by a Unikernel, a Container, or any other future technology). Based on this, the O-CU requires three VMs, and the O-DU requires five VMs, which can be hosted on one or multiple PMs in O-Cloud #1 and O-Cloud #2, respectively.

Each VNFC, $f_i \in \mathcal{C} \cup \mathcal{D}$ requires a certain amount of virtual compute and storage resources, denoted by C_i^{req} and S_i^{req} , respectively. The total required virtual compute and storage

resources of an O-CU and O-DU are obtained by:

$$\mathbb{T}_{com}^{req} = \underbrace{\sum_{i=1}^3 C_i^{req}}_{\text{compute resource of O-CU}} + \underbrace{\sum_{i=4}^8 C_i^{req}}_{\text{compute resource of O-DU}} \quad (1)$$

and

$$\mathbb{T}_{sto}^{req} = \underbrace{\sum_{i=1}^3 S_i^{req}}_{\text{storage resource of O-CU}} + \underbrace{\sum_{i=4}^8 S_i^{req}}_{\text{storage resource of O-DU}}, \quad (2)$$

respectively.

It is worth noting that the relationship between the O-DU and O-CU is many-to-one; thus, $\sum_{i=1}^3 C_i^{req} \geq \sum_{i=4}^8 C_i^{req}$ and $\sum_{i=1}^3 S_i^{req} \geq \sum_{i=4}^8 S_i^{req}$, aimed at avoiding under-utilization of virtual compute and storage resources in O-Cloud #1. Additionally, (de)coding and (de)modulation are the most compute- and storage-resource-demanding functionalities in an O-RAN slice [9], and they are processed in the upper layers of O-gNB, specifically in the O-CU. Therefore, the O-CU must be provisioned with sufficient virtual resources to efficiently process the lower-layer functionalities of multiple O-DUs.

B. Modeling the Infrastructure Layer

Let $\mathcal{V} = \{v_1, v_2, \dots, v_{m-1}, v_m\}$ be a set of m VMs in the Hypervisor Domain such that the index $m \in \mathbb{N}$, and let $\mathcal{P} = \{p_1, p_2, \dots, p_{n-1}, p_n\}$ be a set of n PMs in the Compute Domain such that the index $n \in \mathbb{N}$. The set \mathcal{V} is abstracted from set \mathcal{P} in both O-Cloud #1 and O-Cloud #2. Each O-Cloud site can consist of a large number of PMs, with each PM

Table I. List of key notations related to the proposed system model

Notation	Description
\mathcal{F}	Set of h physical and virtual functions of an O-RAN slice
\mathcal{C}	Set of VNFCs assigned to O-CU
\mathcal{D}	Set of VNFCs assigned to O-DU
\mathcal{R}	Set of physical functions assigned to O-RU
\mathcal{V}	Set of m VMs in the Hypervisor Domain
\mathcal{P}	Set of n PMs in the Compute Domain
\mathcal{Z}	Set of u rApps in the Non-RT RIC
\mathcal{O}	Set of t tasks that are executed by a set of u rApps in \mathcal{Z}
C_i^{req}	Virtual compute resources required by VNFC $f_i \in \mathcal{F}$
S_i^{req}	Virtual storage resources required by VNFC $f_i \in \mathcal{F}$
\mathbb{T}_{com}^{req}	Total required virtual compute resources of an O-RAN slice
\mathbb{T}_{sto}^{req}	Total required virtual storage resources of an O-RAN slice
C_j^{max}	Maximum virtual compute capacity of VM $v_j \in \mathcal{V}$
S_j^{max}	Maximum virtual storage capacity of VM $v_j \in \mathcal{V}$
C_k^{max}	Maximum physical compute capacity of PM $p_k \in \mathcal{P}$
S_k^{max}	Maximum physical storage capacity of PM $p_k \in \mathcal{P}$
$X_{m,n}$	Matrix representation to the VM placement problem
W_j	Total virtual compute and storage workloads of VM $v_j \in \mathcal{V}$
W_{RAN}	Total virtual compute and storage workloads of an O-RAN slice on O-Cloud #1 and O-Cloud #2
W_k	Total compute and storage workloads of PM $p_k \in \mathcal{P}$
w_1	Weighting coefficient for compute resources
w_2	Weighting coefficient for storage resources
C_k^{ava}	Available compute resources in PM $p_k \in \mathcal{P}$
S_k^{ava}	Available storage resources in PM $p_k \in \mathcal{P}$
C_k^{cap}	Compute resource capacity of PM $p_k \in \mathcal{P}$
S_k^{cap}	Storage resource capacity of PM $p_k \in \mathcal{P}$
C_j^{ava}	Available virtual compute resources in VM $v_j \in \mathcal{V}$
S_j^{ava}	Available virtual storage resources in VM $v_j \in \mathcal{V}$
C_j^{cap}	Virtual compute resource capacity of VM $v_j \in \mathcal{V}$
S_j^{cap}	Virtual storage resource capacity of VM $v_j \in \mathcal{V}$
ψ	Resource wastage of PM $p_k \in \mathcal{P}$
ζ	Virtual resource wastage of VM $v_j \in \mathcal{V}$

capable of *hosting* a specific number of VMs. The placement of VMs onto PMs within an O-Cloud site presents a complex optimization challenge. The objective of this placement is to optimize certain criteria, such as minimizing the number of active PMs, maximizing energy efficiency, and so on. Due to the vast number of possible placements and the extensive set of optimization objectives, the VM-to-PM placement problem is classified as a nondeterministic polynomial time (NP)-hard optimization problem [10]. As a result, no single efficient algorithm exists to solve this problem comprehensively. Finding an exact algorithmic solution that provides optimal results typically requires a significant amount of time. Therefore, in practical applications, approximate algorithms are often employed to deliver nearly optimal results within more acceptable levels of computation resources and time.

Each VM, $v_j \in \mathcal{V}$ is characterized by a vector of available virtual resources. Specifically, this means that each $v_j \in \mathcal{V}$ has a maximum virtual compute capacity, denoted by C_j^{max} , and a maximum virtual storage capacity, denoted by S_j^{max} . The former represents the compute capacity, and the latter

represents the storage capacity required to support the VNFC $f_i \in \mathcal{F}$. We consider $f_i \in \mathcal{F}$ to be hosted on $v_j \in \mathcal{V}$ if, when activated, it demands a certain amount of C_j^{max} and S_j^{max} .

Likewise, each PM, $p_k \in \mathcal{P}$ has a maximum physical compute capacity, denoted by C_k^{max} , and a maximum physical storage capacity, denoted by S_k^{max} . The former represents the physical resource capacity for computing, and the latter represents the physical resource capacity for storing the VM, $v_j \in \mathcal{V}$ at a given time. If we assume, for the sake of argument, that $p_k \in \mathcal{P}$ hosts only a single VM at a given time, then C_k^{max} and S_k^{max} are virtualized and fully dedicated to C_j^{max} and S_j^{max} , respectively. On the contrary, if $p_k \in \mathcal{P}$ hosts multiple VMs at a given time, C_k^{max} and S_k^{max} are virtualized and dynamically shared among the C_j^{max} and S_j^{max} of the hosted VMs, based on an optimal resource allocation algorithm.

We now define a variable to represent the placement of VM(s) onto PM(s). To that end, let us assume that $X_{m,n}$ is an adjacency matrix representation to the VM placement problem, defined as follows:

$$X_{m,n} = \begin{bmatrix} x_{1,1} & x_{1,2} & \cdots & x_{1,n-1} & x_{1,n} \\ x_{2,1} & x_{2,2} & \cdots & x_{2,n-1} & x_{2,n} \\ \vdots & \vdots & \ddots & \vdots & \vdots \\ x_{m-1,1} & x_{m-1,2} & \cdots & x_{m-1,n-1} & x_{m-1,n} \\ x_{m,1} & x_{m,2} & \cdots & x_{m,n-1} & x_{m,n} \end{bmatrix},$$

where $x_{j,k}$ is the matrix variable with a double subscript notation that indicates the position of an element in $X_{m,n}$. The first subscript (j) refers to the row that corresponds to the position of a VM in a list of m VMs. The second subscript (k) refers to the column that represents the position of a PM in a list of n PMs.

In such a case, if a single VM is placed on a single PM, the VM placement problem can be defined as follows [2]:

$$\sum_{k=1}^n x_{j,k} = 1, \quad \forall j : 1 \leq j \leq m, \quad (3)$$

where $x_{j,k} \in \{0, 1\}$, $1 \leq j \leq m$, $1 \leq k \leq n$ is 1 if VM, v_j is placed on PM, p_k , and 0 otherwise. However, if multiple VMs are assigned to a single PM, the placement problem is presented in the following [2]:

$$\sum_{j=1}^m x_{j,k} \leq t_k, \quad \forall k : 1 \leq k \leq n, \quad (4)$$

where t_k is the maximum number of VMs, PM, p_k can host. Hence, the placement of $v_j \in \mathcal{V}$ onto $p_k \in \mathcal{P}$ can be presented as a function $f : \mathcal{V} \rightarrow \mathcal{P}$ in such a way that a set of optimization objectives are achieved and a set of constraints are satisfied. Based on this, we formulate the VM placement problem as follows:

$$x_{j,k} = \begin{cases} 1, & \text{if VM } v_j \text{ is placed onto PM } p_k \\ 0, & \text{otherwise.} \end{cases} \quad (5)$$

In both of the above cases, the virtual compute resource demand of VM(s) must not exceed the physical compute

resource capacity of the host PM:

$$\sum_{j=1}^m C_j^{max} x_{j,k} \leq C_k^{max} y_k, \quad \forall k : 1 \leq k \leq n, \quad (6)$$

where C_j^{max} is the virtual compute resource demand by VM, v_j , C_k^{max} is the physical compute capacity offered by PM, p_k , and y_k is 1 if PM p_k is active and 0 otherwise. Likewise, the virtual storage resource demand of VM(s) must not exceed the physical storage resource capacity of the host PM:

$$\sum_{j=1}^m S_j^{max} x_{j,k} \leq S_k^{max} y_k, \quad \forall k : 1 \leq k \leq n, \quad (7)$$

where S_j^{max} is the virtual storage resources demand by VM, v_j , S_k^{max} is the physical storage capacity offered by PM, p_k , and y_k is 1 if PM p_k is active and 0 otherwise.

Although the primary focus of this paper is to examine the interrelationship between VNFCs and VMs, the VM-PM placement problem remains highly relevant to the VNFC-to-VM mapping. Accordingly, we provide the mathematical description of the VM-PM placement in Appendix D.

C. Modeling the Management and Orchestration Layer

In this layer, alongside other management and orchestration components that may exist within or beyond the SMO framework, a large set of rApps can also be placed. Let $\mathcal{Z} = \{z_1, z_2, \dots, z_{u-1}, z_u\}$ represent a set of u rApps within the SMO framework, where the index $u \in \mathbb{N}$. Each rApp $z_l \in \mathcal{Z}$ enables the intelligent control and optimization of certain tasks, providing policy-based guidance to the components of the O-RAN architecture on a control loop with a timescale of $t \geq 1$ second. We assume there exists a set $\mathcal{O} = \{o_1, o_2, \dots, o_{t-1}, o_t\}$ of t tasks, such that the index $t \in \mathbb{N}$, representing the intelligent control and optimization tasks within O-RAN that can be performed by set \mathcal{Z} . Each optimization task $t_g \in \mathcal{O}$ is executed by at least one rApp $z_l \in \mathcal{Z}$.

From a task execution perspective, we believe there could be two types of rApps in set \mathcal{Z} : Single-Task and Multi-Task.

- Single-Task rApps perform one specific optimization task of $t_g \in \mathcal{O}$. They focus on delivering a specialized, streamlined experience, often excelling in their particular domain. These rApps are used when a user requires a dedicated tool for a specific purpose, offering simplicity, efficiency, and ease of use without the added complexity of additional features.
- Multi-Task rApps execute multiple optimization tasks, included in set \mathcal{O} , within the Non-RT RIC. They integrate various features, allowing users to accomplish a range of activities without needing to switch between different rApps. These rApps are often versatile, catering to diverse user needs, and they aim to enhance productivity by consolidating multiple tasks into a unified user experience.

SliceMapper, which is placed in the Management and Orchestration Layer, as illustrated on the upper side of Figure 1, is a member of set \mathcal{Z} . It can function as either a Single-Task or a Multi-Task rApp, performing a certain number of tasks from set \mathcal{O} . The goal of SliceMapper is to find an

optimal solution for mapping the VNFCs in subsets \mathcal{C} and \mathcal{D} of set \mathcal{F} onto specific VMs in set \mathcal{V} , such that a predefined set of optimization objectives (discussed in Section III-A) is achieved and a set of constraints (discussed in Section III-B) is fulfilled. SliceMapper is not responsible for placing the VMs in set \mathcal{V} onto PMs in set \mathcal{P} . We consider this task, which has been extensively examined in the literature [2], to be executed by a resource manager, such as the virtualized infrastructure manager (VIM) in network function virtualization-management and orchestration (NFV-MANO). However, the resource manager can leverage the output of SliceMapper to efficiently and intelligently partition the resources of PMs in set \mathcal{P} , dynamically allocating only the required virtual resources to VMs in set \mathcal{V} to host the corresponding VNFCs of an O-RAN slice in subsets \mathcal{C} and \mathcal{D} of set \mathcal{F} . As a result, the output of SliceMapper helps prevent both over-utilization and under-utilization of resources in O-Cloud sites.

III. PROBLEM FORMULATION OF SLICEMAPPER

Building on the system model defined in the previous section, this section formulates the optimization problem that SliceMapper aims to solve. It first defines the key objective function targeted by SliceMapper, then presents the linear programming formulation of the optimization problem as well as the corresponding constraints.

A. Key Objective Function of the Optimization Problem

Before defining the objective function for the optimization problem that SliceMapper seeks to solve, let us first examine the nature of the problem. Mathematically, the goal of the SliceMapper is to map each VNFC in the Network Function Layer onto a unique VM in the Infrastructure Layer, thereby achieving a one-to-one mapping. In simpler terms, this means that each VNFC must be uniquely hosted by a VM, and each VM can host only one VNFC at a given time. The optimization problem aims to minimize the wastage of both computational and storage resources. Specifically, the objective is to minimize the following expression:

$$(C_j^{max} - C_i^{req}) + (S_j^{max} - S_i^{req}).$$

B. Linear Programming Formulation of the Problem

The linear programming formulation of this optimization problem can be expressed as follows: Let $x_{i,j} \in \{0, 1\}$ be the binary variable, where $x_{i,j} = 1$ if VNFC f_i is placed onto VM v_j , and $x_{i,j} = 0$ otherwise. Based on this, the optimization problem can be formulated as:

$$\text{minimize } \sum_i \sum_j x_{i,j} [(C_j^{max} - C_i^{req}) + (S_j^{max} - S_i^{req})], \quad (8)$$

subject to,

$$\sum_j x_{i,j} = 1, \quad \forall i = 1, \dots, 8, \quad (9)$$

$$\sum_i x_{i,j} \leq 1, \quad \forall j = 1, \dots, m, \quad (10)$$

and

$$x_{i,j} = 0, \quad \text{for } C_i^{req} > C_j^{max} \text{ or } S_i^{req} > S_j^{max}. \quad (11)$$

IV. PROPOSED SOLUTION FOR SLICEMAPPER

Following a detailed discussion on the definition, objectives, and constraints of the optimization problem in the preceding section, we now propose a Q -learning-assisted solution for *SliceMapper* to effectively address these challenges. We begin by formalizing the mapping of O-CU and O-DU onto O-Clouds within the context of Q -learning. Next, we define the process of deriving the optimal mapping policy, which *SliceMapper* is designed to execute. We then define both on-policy and off-policy variants of Q -learning, as well as their implementation using tabular representation and function approximation methods. Furthermore, we analyze the learning rate and exploration rate in optimizing *SliceMapper*'s policy. To derive an optimal policy for *SliceMapper*, we discuss the practical implementation of both on-policy and off-policy variants of the Q -learning algorithm. Each variant is examined using tabular representation and function approximation methods. In total, we present the mathematical foundations and procedural steps for four algorithms aimed at obtaining the optimal policy for *SliceMapper*. Finally, we summarize the key notations associated with the core concepts and tools of the proposed Q -learning algorithms in Table II.

A. Overview of Q -Learning-based Solution for VNF Mapping

Consider a set of n PMs virtualized into a set of m VMs. Each VM $v_j \in \mathcal{V}$, configured with specific amounts of virtual storage and compute resources, can host a single VNFC $f_i \in \mathcal{F}$ at any given time. The resource capacities of the VMs in \mathcal{V} vary and are allocated randomly. The *agent* (i.e., *SliceMapper*¹) receives a request to map a VNFC $f_i \in \mathcal{F}$ onto a VM $v_j \in \mathcal{V}$. During the mapping process, all VMs in \mathcal{V} are categorized into four distinct classes: the *occupied* VM, the *available* VM, the *primary* VM, and the *target* VM. An occupied VM is one that is already hosting a VNFC, and it is therefore forbidden to map another VNFC onto it. An available VM has not yet been assigned to any VNFC. Available VMs are further classified into two types: *sufficient* and *insufficient*. A sufficient VM possesses storage and computational resources that are equal to or greater than those required by a VNFC, whereas an insufficient VM lacks the necessary resources. A primary VM is either an available or occupied VM from which the *SliceMapper* initiates the mapping process. Finally, a target VM is a sufficient, available VM onto which the *SliceMapper* maps the desired VNFC. Within the context of our optimization problem, the critical role of the *SliceMapper* is to determine an optimal *policy* for selecting an appropriate target VM, starting the search from a designated primary VM.

To derive an optimal policy, we utilize Q -learning, one of the most widely employed RL algorithms in the literature. Q -learning involves a dynamic interaction between an agent and its *environment*. The agent acts as a decision-maker that senses its current *state*, adheres to specific policies, and performs *actions* accordingly [11]. The environment encompasses everything external to the agent. In this article,

SliceMapper functions as the agent. The sets \mathcal{F} , \mathcal{V} , the mapping from \mathcal{F} onto \mathcal{V} , and various associated functionalities and elements of the system model (as illustrated in Figure 1) are considered components of the environment.

Within the environment, the state is a fundamental concept that defines the agent's status relative to its surroundings. An environment may consist of several states, with the complete set (finite or infinite) of all states referred to as the *state space*, denoted by $\mathcal{S} = \{s_1, s_2, s_3, \dots\}$. Within the context of the VNFC mapping, the set \mathcal{V} represents the state space, with each VM regarded as an individual state. Each state (i.e., VM) in the state space \mathcal{V} is represented by the 2-tuple $(x_j, y_j) \in S_j^{\max} \times C_j^{\max}$, which encapsulates all relevant information about the VM. The first component, x_j , denotes the storage resources of the VM, while the second component, y_j , denotes its computational resources. Each state contains all essential information about its environment that *SliceMapper* requires to make informed decisions at a given time. This information may include the VM's status (e.g., available or occupied), its virtual compute and storage capacities, details of any previously hosted VNFCs, *rewards* received, and more. Furthermore, *SliceMapper* may or may not store states and their associated information. In Markov systems, such memory storage is unnecessary because the agent only requires knowledge of the current state to act optimally. However, in non-Markov systems, the agent stores states in memory, which enables it to recall state information at any point during the learning process [11].

For each state $s \in \mathcal{S}$, *SliceMapper* can perform a specific set of actions. The set of all possible actions is referred to as the *action space*, denoted by $\mathcal{A}(s) = \{a_1, a_2, a_3, \dots\}$. The action space may vary between states, meaning different states can have different available actions. When the agent takes an action, it may transition from one state to another in a process known as *state transition*. For example, if the agent is at the state s_2 and selects the action a_3 , it transitions to the state s_5 . This process can be expressed as $s_2 \xrightarrow{a_3} s_5$. State transitions can be either deterministic or stochastic and are described by conditional probability distributions [11].

Within the context of our system model, an action corresponds to selecting a VM on which a requested VNFC is to be placed. In a given O-RAN slice, there are 8 VNFCs, and the target O-Cloud site hosts m available VMs. Each VNFC can potentially be placed on any of the m VMs, resulting in m possible actions per VNFC. Therefore, the overall action space of the system model is a *discrete action space* of size $\#\mathcal{A}(s) = 8m$, where each action represents a specific mapping of a VNFC to a VM. For example, if there are 8 VNFCs to be placed and 100 available VMs, then each VNFC has 100 placement options. Consequently, the total number of actions in the action space $\mathcal{A}(s)$ is $8 \times 100 = 800$.

Another critical element within the environment is the *policy*, which guides the agent in deciding which actions to take at each state [11]. A policy is usually denoted by π , where $\pi(a|s)$ represents the probability of taking action a when in state s . Policies can be either deterministic or stochastic. A deterministic policy directly maps each state to a specific action: $\pi(s) = a$, where a is the action chosen at the state s . In

¹The terms *agent* and *SliceMapper* are used interchangeably.

contrast, a stochastic policy defines a probability distribution over possible actions for each state: $\pi(a|s) = p(a|s)$, where $p(a|s)$ is the probability of taking action a in state s .

The ultimate goal of the `SliceMapper` is to determine an *optimal* policy that guides it to the target VM without selecting occupied VMs or taking unnecessary detours. An optimal policy is the one that maximizes the expected cumulative reward the `SliceMapper` receives from any state over the given time, which is the objective of any RL algorithms, including Q -learning. A policy π is considered to be optimal and is denoted as π^* if:

$$\pi^*(s) = \arg \max_{\pi} V_{\pi}(s), \quad (12)$$

where $V_{\pi}(s)$ is the *value function*, which represents the expected *return* (discussed later) when starting at state s and following policy π thereafter. In deterministic environments, a single optimal policy typically exists. In contrast, stochastic environments may allow for multiple policies that may be equally optimal. In essence, a policy defines *ways to act*, and an optimal policy represents *the best way to act*.

When the agent takes an action at a given state, it receives feedback from the environment in the form of a reward, denoted by r . This reward depends on both the state s and the action a , and can therefore be expressed as $r(s, a)$. The set of all rewards $r(s, a)$ for any given state s and action a is called the *reward space* and is denoted by $\mathcal{R}(s, a)$. The reward value can be positive, negative, or zero, each having a distinct impact on the policy the agent learns. Rewards can be deterministic or stochastic, with the conditional probability $p(r|s, a)$ describing the reward process [11].

Within the context of our system model, rewards play a pivotal role by providing feedback to the `SliceMapper` after each action, indicating the effectiveness of the action in contributing to the global objective. Specifically, the reward signals whether the action was beneficial or detrimental in terms of minimizing resource wastage. In our system model, we employ a global wastage-based reward function, which quantifies the change in overall resource surplus following each action. The function is defined as follows:

$$S_{\text{waste}} = 1 - \frac{S_i^{\text{req}}}{S_j^{\text{max}}}$$

and,

$$C_{\text{waste}} = 1 - \frac{C_i^{\text{req}}}{C_j^{\text{max}}}$$

and the reward is computed as

$$R = S_{\text{waste}} + C_{\text{waste}},$$

where R denotes the resulting reward. This formulation captures the impact of each individual VNFC-to-VM placement on the overall system efficiency. A positive reward indicates a reduction in resource wastage, a negative reward indicates an increase in the resource wastage, and a zero reward indicates no change in the overall wastage.

By following a policy, the agent generates a *trajectory*, which is crucial for understanding the agent's movement from a primary state to a target state and the rewards obtained

along the way. A trajectory is essentially a sequence of states, actions, and rewards. In a trajectory, the total rewards accumulated by the agent across all states are referred to as the return. This metric is used to evaluate the policy for finite-length trajectories within Q -learning. However, not all trajectories are finite in length. For infinitely long trajectories, the concept of *discounted return* is used to evaluate a policy. The discounted return represents the sum of all *discounted rewards* and is defined as [11]:

$$G_t = R_{t+1} + \gamma R_{t+2} + \gamma^2 R_{t+3} + \dots = \sum_{k=0}^{\infty} \gamma^k R_{t+k+1}, \quad (13)$$

where G_t is the discounted return starting at time step t , R_{t+k+1} denotes the discounted reward received $k+1$ steps after time t , and $\gamma \in (0, 1)$ is the *discount rate* (or the *discount factor*). Note that R is a random variable such that $R \in \mathcal{R}(s, a)$. The discount rate determines the relative importance of future rewards compared to immediate rewards. The factor γ is applied to each reward in the trajectory. If γ is close to 0, the agent prioritizes immediate rewards, resulting in a shortsighted policy. Conversely, if γ is close to 1, the agent places greater emphasis on future rewards, leading to a farsighted policy.

To simplify summation, G_t can be expressed recursively as:

$$G_t = R_{t+1} + \gamma(R_{t+2} + \gamma R_{t+3} + \dots). \quad (14)$$

Notice that the term in parentheses is exactly G_{t+1} . Thus:

$$G_t = R_{t+1} + \gamma G_{t+1}, \quad (15)$$

which shows the relationship between the current return G_t , the discount factor γ , and the subsequent return G_{t+1} . In cases where rewards are constant (e.g., $R_{t+k+1} = R$), G_t simplifies to an infinite geometric series:

$$G_t = R \cdot \frac{1}{1 - \gamma}, \quad \text{for } \gamma \in (0, 1). \quad (16)$$

For scenarios involving delayed rewards, where contributions to G_t begin after a fixed number of steps (e.g., after 3 steps), G_t can be represented as:

$$G_t = \gamma^3 \cdot \frac{R}{1 - \gamma}, \quad (17)$$

where γ^3 accounts for the delay in the reward accumulation. This formulation emphasizes the importance of γ and its role in weighting future rewards over time.

Finally, another important concept within the environment is the *episode* (or a *trial*), typically considered a finite-length trajectory. An episode records the actions and states the `SliceMapper` progresses through from a starting state to an ending state. In a stochastic environment or policy, starting from the same state can lead to different episodes due to inherent randomness. In contrast, in a deterministic setting, initiating from the same state produces the same episodes.

B. Optimal Action Value, Optimal Policy, and Bellman Optimality Equation for *SliceMapper*

We previously introduced the concept of return G_t as a measure to evaluate policies. While this approach is effective in deterministic systems, it becomes less applicable in stochastic environments due to the inherent variability of outcomes. To address this challenge, the concepts of *state value* and *action value* are introduced as metrics for evaluating the optimality of a policy in stochastic environments. Some RL algorithms rely on state value, while others use action value. In Q -learning, the focus is on action value, making it the central metric discussed in this section.

The action value (or Q -value) is a critical metric in RL. It quantifies the expected return of taking a specific action a at a given state s , followed by adhering to a particular policy π . Formally, the action value (also referred to as the state-action value function) of a state-action pair under policy π , denoted $Q_\pi(s, a)$, is defined as [11]:

$$Q_\pi(s, a) = \mathbb{E}_\pi [G_t | S_t = s, A_t = a], \quad (18)$$

where \mathbb{E}_π represents the expectation under the policy π , S_t is the initial state, A_t is the initial action, and t is the given time step. Using the recursive form of G_t provided in Equation (15) and substituting it into Equation (18), we derive the recursive form of the action value:

$$Q_\pi(s, a) = \mathbb{E}_\pi [R_{t+1} + \gamma G_{t+1} | S_t = s, A_t = a], \quad (19)$$

where R_{t+1} is the reward obtained after taking action a in state s . Moreover, if we define $V_\pi(s)$ as the state value function, the state value for G_{t+1} becomes $V_\pi(S_{t+1})$. Substituting this into Equation (19) leading to:

$$Q_\pi(s, a) = \mathbb{E}_\pi [R_{t+1} + \gamma V_\pi(S_{t+1}) | S_t = s, A_t = a], \quad (20)$$

where $V_\pi(S_{t+1})$ represents the expected value of the next state.

In Q -learning, the primary objective is to determine the optimal action-selection policy π^* that maximizes the expected return. The optimal state-action value function is defined as:

$$Q^*(s, a) = \max_\pi Q_\pi(s, a). \quad (21)$$

This function can be expressed using the following Bellman optimality equation in terms of action values:

$$Q^*(s, a) = \mathbb{E} [R_{t+1} + \gamma \max_a Q^*(S_{t+1}, a) | S_t = s, A_t = a], \quad (22)$$

where $\max_a Q^*(S_{t+1}, a)$ represents the maximum expected return from the next state S_{t+1} , considering all possible actions a . This equation forms the foundation of Q -learning, as it recursively relates the optimal action value of a state-action pair to the rewards and subsequent optimal action values.

The Q -learning is a fundamental algorithm to solve the Bellman optimality equation (see Equation [22]) within the context of *SliceMapper*. Q -learning is a cornerstone algorithm in RL, valued for its model-free nature, off-policy learning approach, simplicity, accessibility, and theoretical guarantee for convergence. Unlike many other RL algorithms, Q -learning specifically targets the estimation of optimal action values and the derivation of optimal policies by iteratively refining the action-value function. This property makes it particularly

Table II. List of key notations related to the proposed RL-assisted framework

Notation	Description
\mathcal{S}	State space, the set of all possible states in which the <i>SliceMapper</i> can exist within the environment
S_t	State at time step t , the t^{th} state in the state space \mathcal{S}
s	Arbitrary state, any state in the state space \mathcal{S}
$\mathcal{A}(s)$	Action set, the set of all possible actions that <i>SliceMapper</i> can take in a given state $s \in \mathcal{S}$
A_t	Action at time step t , the t^{th} action in the action space $\mathcal{A}(s)$
a	Arbitrary action, any action in the action space $\mathcal{A}(s)$
R_t	Reward at time step t , the t^{th} reward in reward space \mathcal{R}
G_t	Discounted return starting at time step t , representing the cumulative discounted rewards from time step t onward
r	Arbitrary reward, any reward in the reward space \mathcal{R}
$\mathcal{R}(s, a)$	Reward space, the set of all possible rewards that the <i>SliceMapper</i> can receive
$p(s' s, a)$	State transition probability, the probability of transitioning from state s to state s' given action $a \in \mathcal{A}$
$p(r s, a)$	Reward distribution, the probability distribution of reward r given a state-action pair (s, a)
$\pi(a s)$	Policy, the probability distribution over actions given state s
\mathbb{E}_π	Expectation under policy π , denoting the expected value of a function when actions are selected according to π .
π^*	Optimal policy, a policy that maximizes cumulative reward
$Q_\pi(s, a)$	State-action value under policy π , the expected cumulative reward for taking action a in state s and then following π
$Q^*(s, a)$	Optimal state-action value function, the expected cumulative reward for taking action a in state s and then following π^*
γ	Discount factor, where $0 < \gamma < 1$
α	Learning rate, where $0 \leq \alpha \leq 1$
ϵ	Exploration rate in an ϵ -greedy policy, where $0 \leq \epsilon \leq 1$
π_b	Behaviour policy, a π used to generate actions during training
π_T	Target policy, a π being optimized and evaluated
$Q_0(s, a)$	Initial Q -value for the state-action pair (s, a) , representing the starting estimate of the action-value function
$\hat{Q}(s, a)$	Approximated Q -value function, an estimate of the true $Q(s, a)$ obtained using function approximation

suitable for solving stochastic optimization problems, such as those encountered in *SliceMapper*.

C. On-Policy and Off-Policy Variants of Q -Learning

The Q -learning algorithm is inherently off-policy. However, it can be applied in both on-policy and off-policy settings [11]. In the on-policy approach, the behavior policy π_b , which generates experience samples, is the same as the target policy π_T , which is continuously updated to converge to an optimal policy. Conversely, in the off-policy approach, these two policies differ. Moreover, in off-policy—widely considered the standard approach to Q -learning—the agent learns the optimal action-value function Q^* independently of the policy used for exploration. This means that Q -learning updates its Q -values using the maximum estimated Q -value of the next state (i.e., the greedy action), rather than the action taken by the current policy. This independence is what classifies Q -learning as an off-policy method. In contrast, on-policy Q -learning updates its Q -values based on the action actually executed by the current policy, rather than the greedy action. This version of Q -learning is closely associated with state action reward state

action (SARSA) algorithm and represents a slight variation of the standard off-policy Q -learning approach.

D. Tabular Representation and Function Approximation

The aforementioned two variants of Q -learning can employ either the tabular representation method or the function approximation method to represent the action-value function, policy, or other key components of the Q -learning algorithm.

In the tabular method, a table is used to explicitly store and update the action-value function for each state-action pair. This table maps every state-action pair (s, a) to its corresponding estimated value $Q(s, a)$. The approach is generally suitable when the state-action space is small and discrete. This method enables an accurate representation of the action-value function, as each state-action pair has a dedicated entry, and it converges to the true value with sufficient exploration and updates. However, it also has certain limitations. Specifically, the tabular method becomes impractical for large or continuous state-action spaces due to memory and computational constraints. Additionally, it lacks generalization to unseen states, requiring every state to be explicitly explored and stored.

The function approximation method employs parameterized functions (e.g., neural networks, linear regression models, or other parametric/non-parametric models) to estimate the action-value function. Instead of using a table, a function \hat{Q} approximates the mapping: $Q(s, a) \approx \hat{Q}(s, a)$ for action-value functions. This approach allows generalization to unseen states or actions and can incorporate complex features and architectures for sophisticated tasks. However, function approximation also has some limitations. First, it may not perfectly model the true action-value function, leading to suboptimal policies. Second, it requires more computational resources and careful selection of the function type, training algorithm, and features. Third, training complex models (e.g., deep neural networks) in RL can be unstable and sensitive to hyperparameters.

E. The Learning Rate and Exploration Rate in Q -Learning

In both tabular and function approximation-based Q -learning, the efficiency and convergence of the learning process are influenced by key parameters. Among these, the *learning rate* (α) and *exploration rate* (ϵ) play a fundamental role in shaping how an agent acquires and refines its policy over time. The learning rate determines the extent to which newly acquired information updates the agent's existing knowledge, while the exploration rate dictates the trade-off between discovering new actions and exploiting known strategies. A well-balanced choice of these parameters is crucial to ensure stable and efficient learning, particularly in complex environments where optimal policies evolve dynamically.

In Q -learning method, the learning rate (α) determines the extent to which newly acquired information updates the existing Q -value. It is constrained by $0 \leq \alpha \leq 1$. When $\alpha = 0$, the Q -value remains unchanged, whereas $\alpha = 1$ fully replaces it with the new estimate. For $0 < \alpha < 1$, the update follows a weighted interpolation between the old and new estimates. A smaller α (e.g., 0.1) results in slower but more stable learning, while a larger α (e.g., 0.9) accelerates

learning at the cost of increased variance. Proper tuning of α is crucial for convergence to optimal Q -values.

The exploration rate ϵ is a crucial hyperparameter that controls the balance between *exploration* (trying new actions) and *exploitation* (choosing the best-known action based on learned Q -values). The value of ϵ typically lies within the range $[0, 1]$ and is a key component of the ϵ -greedy policy. Under this policy—one of the most commonly used action-selection mechanisms—the agent selects a random action with probability ϵ (exploration) and chooses the action with the highest estimated Q -value with probability $1 - \epsilon$ (exploitation). Mathematically, the action a_t at time step t is chosen as:

$$a_t = \begin{cases} \text{random action,} & \text{with probability } \epsilon, \\ \arg \max_a Q(s_t, a), & \text{with probability } 1 - \epsilon. \end{cases}$$

To balance exploration and exploitation throughout the learning process, a common strategy is to gradually decay ϵ over time using predefined decay schedules (e.g., linear, exponential, or inverse-time decay). This ensures that the agent explores more (i.e., ϵ is high) in the initial stages of training, allowing it to discover optimal strategies, and exploits more (i.e., ϵ is low) in later stages as it gains confidence in its learned Q -values. It is important to note that maintaining a high ϵ value (e.g., $\epsilon = 1.0$ for too long) can result in excessive exploration, leading to slow convergence. Conversely, setting ϵ too low from the beginning (e.g., $\epsilon = 0.01$) may cause the agent to converge prematurely to a suboptimal policy. Therefore, an appropriate decay strategy is essential to achieve an optimal balance, enabling the agent to explore sufficiently early on while eventually prioritizing exploitation as learning progresses. Lastly, it should be noted that if $\epsilon = 0$, the ϵ -greedy policy reduces to a purely greedy policy, which should be avoided in the case of on-policy variants.

Algorithm 1 On-Policy Q -Learning (Tabular Representation Method) for Learning Q^* and π^*

```

1: Input Parameters:
2:  $\mathcal{S}, \mathcal{A}(s), \mathcal{R}(s, a)$ 
3: Number of episodes  $N \in \mathbb{N}$  for which Algorithm 1 terminates
4:  $0 < \gamma < 1; 0 \leq \epsilon \leq 1; 0 \leq \alpha_t \leq 1, \forall (s, a) \in \mathcal{S} \times \mathcal{A}$ 
    $\forall t \in \{0, 1, \dots, N\} \in \mathbb{N}$ 
5: Initial state-action value set to  $Q_0(s, a) = 0, \forall (s, a)$ 
6: An initial  $\epsilon$ -greedy  $\pi_0$  derived from  $Q_0$ 
7: Output:
8: Learn optimal  $Q$ -values  $Q^*$ , where  $\epsilon$ -greedy( $Q^*$ )  $\approx \pi^*$ 
9: Learn optimal policy  $\pi^*$  that maximizes cumulative rewards
10: Algorithm:
11: Initialize  $Q_0$  for all  $(s, a)$ 
12: while non-converged do
13:   Initialize  $S_0$ 
14: end while
15: for each episode do
16:   while  $S_t$  for  $t \in \{0, 1, \dots, N\} \in \mathbb{N}$  is not terminal state do
17:     Collect the experience sample of the form  $(A_t, R_{t+1}, S_{t+1})$ 
18:     Update  $Q$ -value for  $(S_t, A_t)$ : Use Equation (23)
19:     Update policy for  $S_t$ :
20:     if  $a = \arg \max_a Q_{t+1}(S_t, a)$  then
21:       Use Equation (24)
22:     else
23:       Use Equation (25)
24:     end if
25:   end while
26: end for
27: return the pair  $(Q^*, \pi^*)$ 

```

F. Q-Learning Algorithm Using Tabular Representation

Building upon the preceding discussions, we now introduce the on-policy and off-policy methods of Q-learning using the tabular representation approach. The pseudocodes for both variants of Q-learning are presented and discussed below, as shown in Algorithm 1 and Algorithm 2, respectively.

1) On-Policy Q-Learning Using Tabular Representation:

As outlined in Algorithm 1, this algorithm focuses on learning optimal policy π^* by directly improving the policy being followed during the learning process.

Algorithm 2 Off-Policy Q-Learning (Tabular Representation Method) for Learning Q^* and π^*

```

1: Input Parameters:
2:    $\mathcal{S}, \mathcal{A}(s), \mathcal{R}(s, a)$ 
3:   Number of episodes  $N \in \mathbb{N}$  for which Algorithm 2 terminates
4:    $0 \leq \alpha_t \leq 1, \forall (s, a) \in \mathcal{S} \times \mathcal{A}$  and  $\forall t \in \{0, 1, \dots, N\} \in \mathbb{N}; 0 < \gamma < 1$ 
5:   Behaviour policy  $\pi_b(a|s), \forall (s, a)$ 
6:   Initial state-action value set to 0 [i.e.,  $Q_0(s, a) = 0, \forall (s, a)$ ]
7: Output:
8:   Learn optimal state-action values  $Q^*$  and an optimal policy  $\pi^*$  for all states, derived from the experience samples generated by the behavior policy  $\pi_b$ 
9: Algorithm:
10: Initialize  $Q_0$  for all  $(s, a)$ 
11: while non-converged do
12:   Initialize  $S_0$ 
13: end while
14: for each episode do
15:   while  $S_t$  for  $t \in \{0, 1, \dots, N\} \in \mathbb{N}$  is not terminal state do
16:     Collect the experience sample of the form  $(A_t, R_{t+1}, S_{t+1})$  generated by the behavior policy  $\pi_b$ 
17:     Update  $Q$ -value for  $(S_t, A_t)$ : Using Equation (23)
18:     Update policy for  $S_t$ :
19:     if  $a = \arg \max_a Q_{t+1}(S_t, a)$  then
20:       Use Equation (26)
21:     else
22:       Use Equation (27)
23:     end if
24:   end while
25: end for
26: return the pair  $(Q^*, \pi^*)$ 

```

In the input, we consider the state space \mathcal{S} , the action space $\mathcal{A}(s)$, and the reward space $\mathcal{R}(s, a)$. In addition, key parameters such as the discount factor γ , exploration rate ϵ , and learning rate α_t are included. A predetermined value $N \in \mathbb{N}$ (e.g., $N = 100$), which defines the maximum number of episodes before the algorithm terminates, is also taken into account. Given these input parameters, we initialize the Q -table with the initial state-action values $Q_0(s, a) = 0$ for all state-action pairs (s, a) and define an initial ϵ -greedy policy π_0 . Ultimately, for the output, we expect Algorithm 1 to learn an optimal Q -value Q^* and an optimal policy π^* that maximizes the cumulative rewards.

Algorithm 1 begins with an initialization step where we set $Q_0 = 0$. If the algorithm has already converged, the learning process terminates, yielding the optimal pair (Q^*, π^*) . Otherwise, we initialize the initial state S_0 . Next, we enter the main iterative process. Within the `for` loop, we iterate through all states S_t for $t \in \{0, 1, \dots, N\}$. At each episode, we check whether S_t is the target state. If S_t is a terminal state, the algorithm terminates, having achieved (Q^*, π^*) . Otherwise, the agent selects an action A_t based

on the current policy² $\pi_t(S_t)$. The agent then executes the action A_t , receives a reward R_{t+1} , transitions to the next state S_{t+1} , and records the triplet (A_t, R_{t+1}, S_{t+1}) . Subsequently, the Q_{t+1} value is updated using [11]:

$$Q_{t+1}(S_t, A_t) = Q_t(S_t, A_t) - \alpha_t [Q_t(S_t, A_t) - (R_{t+1} + \gamma \max_{a \in \mathcal{A}(S_{t+1})} Q_t(S_{t+1}, a))]. \quad (23)$$

This equation has an equivalent representation using the expectation operator in the Bellman optimality equation (which is provided in Equation [22]). We prove the equivalence of the expectation operator formulation in Appendix E.

Now, we update the policy for the state S_t using ϵ -greediness. If the action $a = \arg \max_a Q_{t+1}(S_t, a)$, the updated policy π_{t+1} is given by [11]:

$$\pi_{t+1}(a|S_t) = 1 - \frac{\epsilon}{|\mathcal{A}(S_t)|} (|\mathcal{A}(S_t)| - 1). \quad (24)$$

Otherwise, we update π_{t+1} using [11]:

$$\pi_{t+1}(a|S_t) = \frac{\epsilon}{|\mathcal{A}(S_t)|}. \quad (25)$$

Finally, Algorithm 1 terminates and returns the optimal pair (Q^*, π^*) .

2) Off-Policy Q-Learning Using Tabular Representation:

As defined in Algorithm 2, the off-policy Q-learning algorithm aims to learn an optimal target policy³, π_T , for all states using experience samples generated by the behavior policy, π_b .

The inputs to the algorithm include \mathcal{S} , $\mathcal{A}(s)$, and $\mathcal{R}(s, a)$. Additionally, the learning rate α_t and a predefined episode limit $N \in \mathbb{N}$ (e.g., $N = 500$) are considered to ensure termination within a finite amount of time. The initial state-action values are set to zero, i.e., $Q_0(s, a) = 0$ for all state-action pairs (s, a) . The behavior policy $\pi_b(a|s)$, defined for all (s, a) , is also provided as input. The algorithm outputs an optimal pair (Q^*, π^*) for any given state, learned from experience samples generated by the behavior policy π_b .

Given the input parameters, we begin Algorithm 2 by initializing the Q -table with state-action values set to zero, i.e., $Q_0(s, a) = 0$ for all state-action pairs (s, a) . We also initialize an initial greedy policy, π_0 . If the algorithm converges on the first attempt, the target policy is reached. Otherwise, the iterative process continues.

Within the looping structure, we collect triplets (A_t, R_{t+1}, S_{t+1}) for all t , iterate through all episodes generated by the behavior policy π_b , and update both the Q -values and the target policy⁴. For each episode $t \in \{0, 1, \dots, N\}$, we update the Q -value for (S_t, A_t) using Equation (23). After updating the Q -values, we update the target policy for S_t as follows:

- If the action $a = \arg \max_a Q_{t+1}(S_t, a)$, the policy is updated using below equation [11]:

$$\pi_{T,t+1}(a|S_t) = 1. \quad (26)$$

- Otherwise, if $a \neq \arg \max_a Q_{t+1}(S_t, a)$, the policy is updated using the following equation [11]:

$$\pi_{T,t+1}(a|S_t) = 0. \quad (27)$$

²In on-policy Q-learning, the agent follows the same policy while learning.

³In off-policy Q-learning algorithms, the target policy π_T and the optimal policy π^* are equivalent and can be used interchangeably.

⁴The policy update follows a greedy strategy in off-policy Q-learning.

Algorithm 3 On-Policy Q -Learning (Function Approximation Method) for Learning Q^* and π^*

```

1: Input Parameters:
2:  $\mathcal{S}, \mathcal{A}(s), \mathcal{R}(s, a)$ 
3: Number of episodes  $N \in \mathbb{N}$  for which Algorithm 3 terminates
4:  $0 \leq \alpha_t \leq 1, \forall (s, a) \in \mathcal{S} \times \mathcal{A}$  and  $\forall t \in \{0, 1, \dots, N\} \in \mathbb{N};$ 
    $0 \leq \epsilon \leq 1; 0 < \gamma < 1$ 
5: Initial  $Q$ -value  $Q_0$  set to 0, i.e.,  $Q_0 = 0$ 
6: Initial  $\epsilon$ -greedy policy  $\pi_0$ 
7: Output:
8: Learn optimal  $Q$ -value  $Q^*$ 
9: Learn optimal policy  $\pi^*$  that maximizes cumulative rewards
10: Algorithm:
11: Initialize  $Q_0 = 0$  for all  $(s, a) \in \mathcal{S} \times \mathcal{A}$ 
12: while non-converged do
13:   Initialize  $S_0$ 
14: end while
15: for each episode do
16:   while  $S_t$  for  $t \in \{0, 1, \dots, N\}$  is not terminal state do
17:     Collect the experience samples of the form  $(A_t, R_{t+1}, S_{t+1})$ 
     given  $S_t$ : it implies generating  $A_t$  according to  $\pi_t(S_t)$  and obtaining
      $R_{t+1}, S_{t+1}$  through interaction with the environment
18:     Update  $Q$ -value for  $(S_t, A_t)$ : Using Equation (28)
19:     Update policy for  $S_t$ :
20:     if  $a = \arg \max_{a \in \mathcal{A}(S_t)} \hat{Q}(S_t, a, Q_{t+1})$  then
21:       Use Equation (26)
22:     else
23:       Use Equation (27)
24:     end if
25:   end while
26: end for
27: return the pair  $(Q^*, \pi^*)$ 

```

At this point, the looping structure terminates, and we return the optimal Q -value and target policy pair (Q^*, π^*) .

G. Q -Learning Algorithm Using Function Approximation

Following a discussion on the on-policy and the off-policy Q -learning algorithms using the tabular representation method, we now examine both variants using the linear function approximation method in this subsection. We provide the pseudocodes for both variants (see Algorithm 3 and Algorithm 4, respectively) and discuss them below.

1) On-Policy Q -Learning Using Function Approximation:

As presented in Algorithm 3, this algorithm aims to learn the optimal policy π^* through the linear function approximation method by iteratively refining the policy being followed during the learning process.

The input parameters considered are $\mathcal{S}, \mathcal{A}(s)$, and $\mathcal{R}(s, a)$, along with an ϵ and an α . We begin with an initial ϵ -greedy policy π_0 and a predetermined number of episodes, $N \in \mathbb{N}$ (e.g., $N = 1000$ episodes⁵). The Q -table is initialized with state-action values set to zero, i.e., $Q_0(s, a) = 0$. Ultimately, Algorithm 3 is expected to learn Q^* and π^* as output.

Algorithm 3 starts by setting $Q_0 = 0$. As with previous algorithms, the first step is to check whether Algorithm 3 has already converged. If it has, the learning process terminates, returning (Q^*, π^*) . Otherwise, we initialize S_0 .

Within the `for` loop, we iterate through all states S_t for $t \in \{0, 1, \dots, N\}$. At each episode, we check whether S_t is the target state. If S_t is a terminal state, the algorithm terminates, having achieved (Q^*, π^*) . Otherwise, the agent selects an action A_t based on the current policy $\pi_t(S_t)$. The agent then

⁵The pair (Q^*, π^*) is optimal when N is sufficiently large.

Algorithm 4 Off-Policy Q -Learning (Function Approximation Method) for Learning Q^* and π^*

```

1: Input Parameters:
2:  $\mathcal{S}, \mathcal{A}(s), \mathcal{R}(s, a)$ 
3: Number of episodes  $N \in \mathbb{N}$  for which Algorithm 4 terminates
4: Behavior policy  $\pi_b(a|s), \forall (s, a)$ 
5:  $0 \leq \alpha_t \leq 1, \forall (s, a) \in \mathcal{S} \times \mathcal{A}$  and  $\forall t \in \{0, 1, \dots, N\} \in \mathbb{N};$ 
    $0 < \gamma < 1$ 
6: Initial  $Q$ -value  $Q_0$  set to 0, i.e.,  $Q_0 = 0$ 
7: Initial policy  $\pi_0$ 
8: Output:
9: Learn optimal state-action values  $Q^*$  and an optimal policy  $\pi^*$  for all
   states, derived from the experience samples generated by the behavior
   policy  $\pi_b$ 
10: Algorithm:
11: Initialize  $Q_0 = 0$  for all  $(s, a) \in \mathcal{S} \times \mathcal{A}$ 
12: while non-converged do
13:   Initialize  $S_0$ 
14: end while
15: for each episode do
16:   while  $S_t$  for  $t \in \{0, 1, \dots, N\}$  is not terminal state do
17:     Collect the experience samples of the form  $(A_t, R_{t+1}, S_{t+1})$ 
     generated by the policy  $\pi_b$ 
18:     Update  $Q$ -value for  $(S_t, A_t)$ : Using Equation (28)
19:     Update policy for  $S_t$ :
20:     if  $a = \arg \max_{a \in \mathcal{A}(S_t)} \hat{Q}(S_t, a, Q_{t+1})$  then
21:       Use Equation (26)
22:     else
23:       Use Equation (27)
24:     end if
25:   end while
26: end for
27: return the pair  $(Q^*, \pi^*)$ 

```

executes the action A_t , receives a reward R_{t+1} , transitions to the next state S_{t+1} , and records the triplet (A_t, R_{t+1}, S_{t+1}) . The Q_{t+1} is then updated using the following equation [11]:

$$Q_{t+1}(S_t, A_t) = Q_t + \alpha_t [R_{t+1} + \gamma \max_{a \in \mathcal{A}(S_{t+1})} \hat{Q}(S_{t+1}, a, Q_t) - \hat{Q}(S_t, A_t, Q_t)] \nabla_Q \hat{Q}(S_t, A_t, Q_t). \quad (28)$$

This equation can also be expressed in terms of the expectation-based Bellman optimality equation as follows:

$$Q^*(s, a) = \mathbb{E} [R_{t+1} + \gamma \max_{a \in \mathcal{A}(S_{t+1})} \hat{Q}(S_{t+1}, a, Q^*) | S_t = s, A_t = a]. \quad (29)$$

The equivalence between Equation (28) and Equation (29) is proven in Appendix F.

After updating Q , we update the policy π for state S_t using ϵ -greedy strategy. If the action $a = \arg \max_a Q_{t+1}(S_t, a)$, the updated policy π_{t+1} is given by Equation (24). Otherwise, we update π_{t+1} using Equation (25). Finally, Algorithm 3 returns the optimal pair (Q^*, π^*) and terminates.

2) Off-Policy Q -Learning Using Function Approximation:

As presented in the pseudocode of Algorithm 4, the off-policy Q -learning algorithm employs a linear function approximation method to learn the optimal target policy, π^* , and the optimal Q -value, Q^* , for all states using experience samples generated by the behavior policy, π_b .

The inputs for this algorithm include the usual $\mathcal{S}, \mathcal{A}(s)$, and $\mathcal{R}(s, a)$. Additionally, α_t, γ , and a predefined episode limit $N \in \mathbb{N}$ are taken into account. We initialize the Q -table with $Q_0(s, a) = 0$ for all state-action pairs. The behavior policy $\pi_b(a|s)$, defined for all (s, a) , is also provided as input to generate experience samples. The algorithm outputs an optimal pair (Q^*, π^*) for any given state, learned from experience samples generated by the behavior policy π_b .

Given the inputs, we begin Algorithm 4 by initializing the Q -table. In addition, the algorithm initializes an initial greedy policy, π_0 . As a first step, we check whether the algorithm has already converged; if so, the target policy has been attained, and the process terminates. Otherwise, we proceed with the iterative process. Within the looping structure, we collect the triplets (A_t, R_{t+1}, S_{t+1}) for all $t \in \{0, 1, \dots, N\}$, where these are the experience samples, precisely generated by the behavior policy π_b . For each episode $t \in \{0, 1, \dots, N\}$, we update the Q -value for (S_t, A_t) using Equation (28).

Subsequently, we update the policy as follows. If the action $a = \arg \max_a Q_{t+1}(S_t, a)$, the policy is updated using Equation (26). Else, if $a \neq \arg \max_a Q_{t+1}(S_t, a)$, the policy is updated according Equation (27). At this point, the looping structure terminates. Finally, we return the optimal Q -value and target policy pair (Q^*, π^*) .

V. PERFORMANCE EVALUATION OF SLICEMAPPER

Building upon the system model and learning formulations introduced in the preceding sections, this section evaluates the performance of SliceMapper using four variants of the Q -learning algorithm. The evaluation aims to analyze the learning behavior, convergence properties, and stability of each variant under a realistic VM–VNFC mapping scenario. We first describe the simulation environment and dataset employed for the experiments, followed by a detailed analysis of the results obtained for each learning method. Finally, a comparative performance assessment is presented to highlight the relative strengths and limitations of the considered approaches.

A. Simulation Setting

All four variants of the Q -learning algorithm were implemented in *Python* using standard scientific computing libraries, including *Random*, *NumPy*, *Matplotlib*, and *Collections*. Each variant was trained for 500 episodes with a fixed learning rate $\alpha = 0.1$, discount factor $\gamma = 0.99$, and exploration rate $\epsilon = 0.1$. The experiments were conducted on a dataset consisting of 8 VNFCs and 100 VMs. Each VNFC is defined by its computational and storage requirements, while each VM is characterized by its corresponding computational and storage capacities. This configuration results in a redundant action space, enabling multiple feasible VNFC–VM mappings with different levels of resource utilization efficiency.

To evaluate the performance of all four learning variants, several metrics were considered: episode versus total reward (reflecting reward evolution over episodes), episode versus episode length (indicating the efficiency of VNFC placement per episode), episode versus exploratory actions (capturing the exploration behavior of the policy), episode versus cumulative reward (representing the total reward accumulated over time), and episode versus exploration ratio (characterizing the long-term learning dynamics of the agent). These metrics collectively provide insights into both short-term learning behavior and long-term policy convergence. A comparative performance analysis of the VNFC–to–VM mapping problem across all four variants is subsequently conducted based on these metrics.

Finally, an additional comparative analysis is performed using the area under the curve (AUC) values derived from the learning curves of each variant. Furthermore, the average reward, standard deviation, and convergence episode are computed to quantitatively assess learning stability, performance consistency, and convergence behavior across the different variants of the Q -learning algorithm.

B. Results Analysis

Based on the four Q -learning variants introduced earlier, this subsection analyzes their performance using the evaluation metrics described above.

1) *On-Policy Tabular Representation*: The learning behavior of the on-policy tabular Q -learning agent over 500 episodes is illustrated in Figures 2–6.

Figure 2 shows drastic fluctuations in the total reward obtained per episode, with values ranging approximately from -1 to 10 . While the agent frequently attains near-optimal rewards (around 10), these episodes are interspersed with instances of significantly lower performance. This behavior suggests that the learned policy does not fully stabilize over the training horizon. Although near-optimal rewards are frequently achieved, the absence of variance reduction over time suggests that the learned policy does not converge to a consistently optimal behavior. The observed high variance can be attributed, at least in part, to the stochastic nature of the environment, which introduces variability in state transitions and reward outcomes.

Figures 3 and 4 provide additional insights into the agent’s learning dynamics. As illustrated in Figure 3, the episode length varies between 2 and 8 steps across training episodes. This variability indicates that the agent struggles to consistently identify and exploit efficient action sequences that minimize the number of steps required to complete the task. The absence of a decreasing trend in episode length further indicates that the agent does not consistently learn minimal-step placement strategies, even when high rewards are obtained. Furthermore, Figure 4 shows the number of exploratory actions per episode. The observed values generally range from 0 to 5 and exhibit a stochastic pattern, indicating sustained exploration throughout the training process. This persistent exploratory behavior, driven by the fixed exploration rate, contributes to the observed variability in episode length and reward, further limiting policy stabilization.

Figures 5 and 6 illustrate the evolution of cumulative reward and exploration ratio over training episodes, respectively. The cumulative reward exhibits an approximately linear increase, indicating that the agent continues to accumulate rewards steadily over time without severe performance degradation. This trend suggests that, despite variability at the episode level, the learning process remains overall progressive. While cumulative reward growth confirms stable learning progress, it does not necessarily imply convergence to an optimal or efficient policy, as episode-level variability remains high. As shown in Figure 6, the exploration ratio remains highly variable throughout training, with no evident decay trend. This behavior reflects the fixed ϵ -greedy exploration strategy, which maintains a constant level of exploration across episodes.

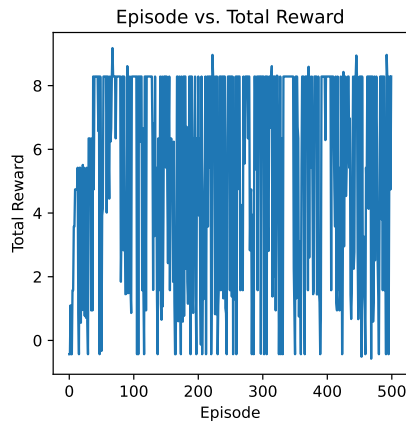


Figure 2. Episode versus total reward for the on-policy tabular Q -learning agent

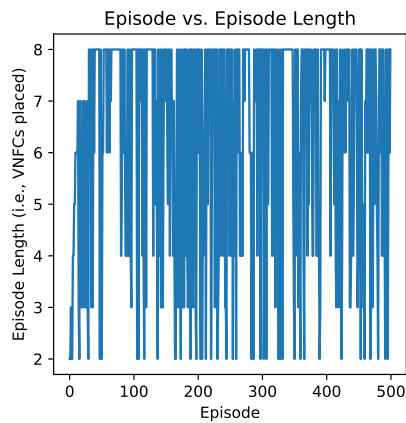


Figure 3. Episode versus episode length for the on-policy tabular Q -learning agent

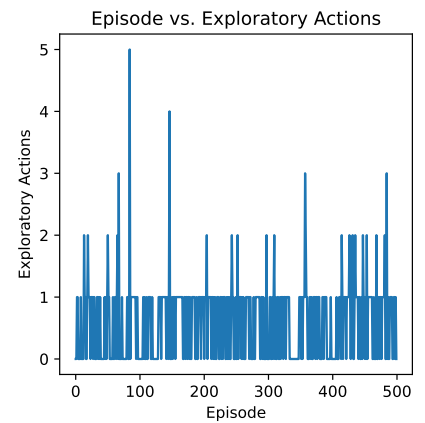


Figure 4. Episode versus exploratory actions for the on-policy tabular Q -learning agent

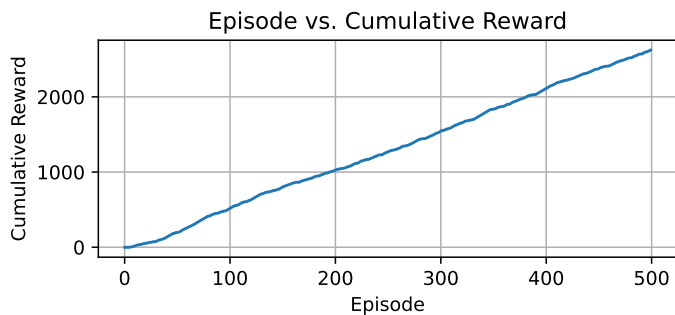


Figure 5. Episode versus cumulative reward for the on-policy tabular Q -learning agent

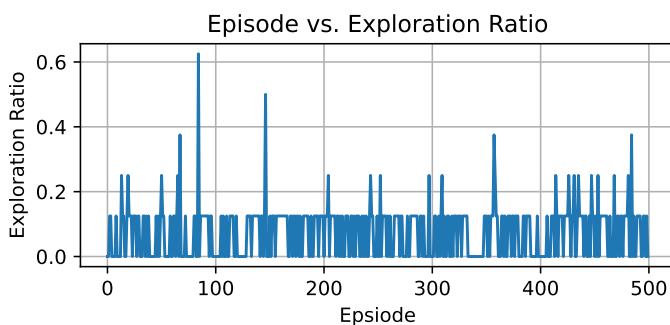


Figure 6. Episode versus exploration ratio for the on-policy tabular Q -learning agent

Therefore, persistent exploration contributes to fluctuations in episode-level performance and prevents full exploitation of the learned policy.

In summary, these results indicate that while the agent is able to steadily accumulate rewards over time, its learning performance remains suboptimal in terms of convergence stability and execution efficiency in complex VNFC-to-VM mapping scenarios. Therefore, further hyperparameter tuning—particularly with respect to the learning rate and exploration strategy—may be required to improve convergence behavior, reduce performance variability, and enhance overall policy efficiency.

2) *Off-Policy Tabular Representation*: The learning behavior of the Q -learning agent following the off-policy tabular representation over 500 episodes is provided in Figures 7–11.

Figure 7 depicts the total reward obtained per episode under

the off-policy tabular Q -learning approach. Similar to the on-policy case, the reward signal exhibits substantial fluctuations, with values ranging approximately from -1 to 9 . The agent frequently attains near-optimal rewards (around 9), indicating its ability to identify high-quality actions under the greedy target policy. However, these high-reward episodes are interspersed with instances of significantly degraded performance, including rewards close to the minimum observed values. This behavior suggests that, although the off-policy learning mechanism enables the agent to discover near-optimal actions, the learned policy does not consistently stabilize across episodes. The high variance in episode-level rewards can be attributed to the stochastic nature of the environment, as well as to the continued exploration induced by the behavior policy, which introduces variability despite updates being performed with respect to a greedy target policy.

Figures 8 and 9 provide additional insights into the learning behavior of the off-policy tabular agent. As illustrated in Figure 8, the episode length varies widely between 2 and 8 steps across training episodes. This pronounced variability indicates that, despite identifying high-reward actions, the agent does not consistently execute efficient action sequences that minimize task completion steps. Figure 9 depicts the number of exploratory actions per episode. The observed values generally remain low, ranging from 0 to 4, while exhibiting a stochastic pattern throughout training. This behavior reflects the use of an exploratory behavior policy in off-policy learning, which continues to introduce variability in action selection even as the target policy remains greedy. As a result, persistent exploration contributes to fluctuations in episode length and limits the consistency of execution efficiency.

Figures 10 and 11 present the evolution of cumulative reward and exploration ratio over training episodes, respectively. The cumulative reward exhibits an approximately linear growth trend, indicating that the off-policy agent continues to accumulate rewards steadily over time. This behavior confirms that learning progresses in aggregate, even though individual episodes may exhibit significant performance variability. As shown in Figure 11, the exploration ratio remains highly variable throughout the training process, with no clear decay or stabilization trend. This reflects the nature of off-

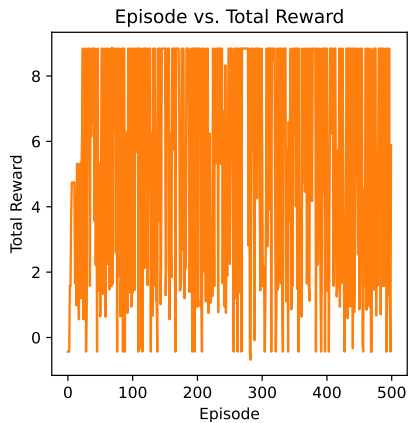


Figure 7. Episode versus total reward for the off-policy tabular Q -learning agent

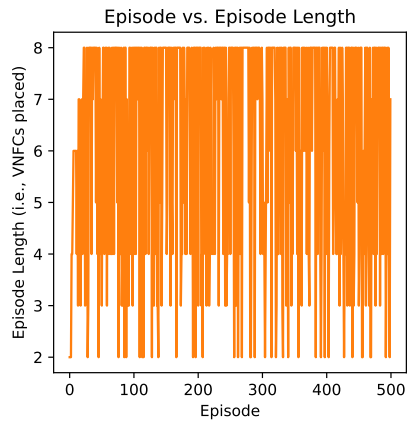


Figure 8. Episode versus episode length for the off-policy tabular Q -learning agent

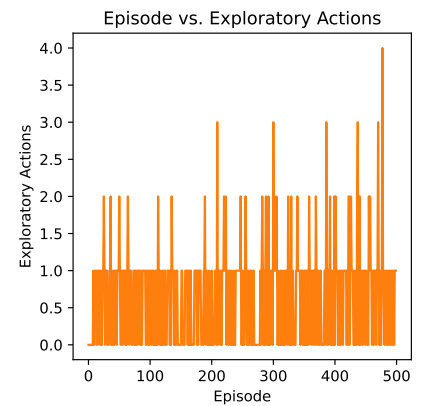


Figure 9. Episode versus exploratory actions for the off-policy tabular Q -learning agent

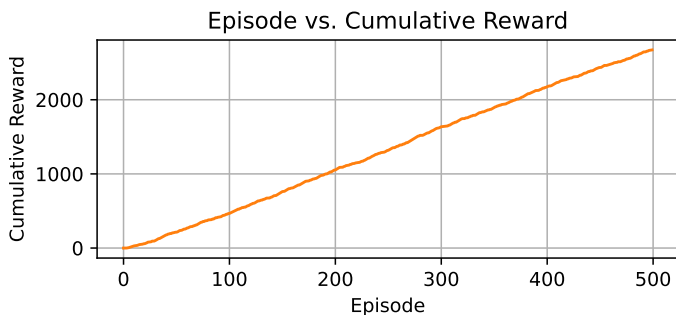


Figure 10. Episode versus cumulative reward for the off-policy tabular Q -learning agent

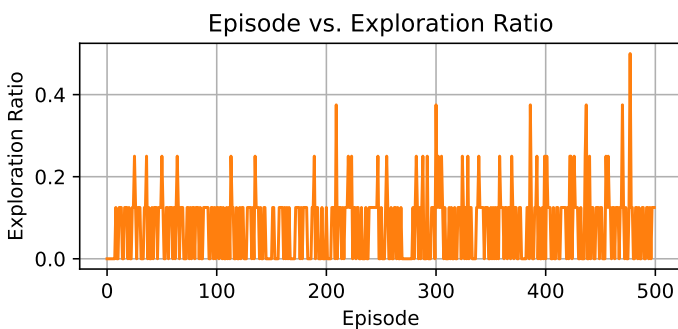


Figure 11. Episode versus exploration ratio for the off-policy tabular Q -learning agent

policy learning, where a greedy target policy is updated while actions are selected according to an exploratory behavior policy. Consequently, the lack of convergence in exploration behavior contributes to persistent fluctuations in episode-level performance, despite steady cumulative reward growth.

Overall, the performance of the off-policy tabular Q -learning approach is sensitive to the selected hyperparameters, particularly those governing learning rate and exploration behavior. Therefore, careful hyperparameter tuning is necessary to improve convergence stability, reduce performance variability, and enhance the robustness of the learned policy.

3) *On-Policy Function Approximation:* The learning dynamics of the on-policy Q -learning agent employing the function approximation method over 500 training episodes are illustrated in Figures 12–16.

Figure 12 illustrates the episode-wise total reward obtained

by the on-policy Q -learning agent with function approximation. The reward signal exhibits stochastic fluctuations across episodes, with values ranging approximately from -1 to 4 . In contrast to the tabular representation methods, the achieved rewards are generally lower, with most episodes concentrated around intermediate reward levels rather than consistently attaining near-optimal outcomes. This behavior can be attributed to the use of function approximation under the considered experimental configuration, which comprises 8 VNFCs and 100 VMs. The resulting action space of 800 possible VNFC-to-VM placement actions increases the complexity of value estimation and amplifies sensitivity to the selected hyperparameters. As a result, near-optimal rewards are achieved only sporadically, and the learned policy does not fully stabilize across episodes. Additionally, the stochastic nature of the environment further contributes to the observed reward variability.

Figures 13 and 14 provide additional insights into the learning behavior of the on-policy agent employing function approximation. As shown in Figure 13, the episode length varies between 2 and 7 steps across training episodes. Compared to the tabular on-policy case, the agent more frequently completes the placement process within a smaller number of steps, indicating improved execution efficiency despite variability in reward magnitude. Figure 14 illustrates the number of exploratory actions per episode. The observed values generally remain low, typically ranging from 0 to 4, while exhibiting a stochastic pattern throughout training. This behavior reflects persistent exploration induced by the fixed ϵ -greedy strategy, which, when combined with function approximation, contributes to continued policy adaptation but also limits full exploitation of learned action-value estimates.

Figure 15 illustrates the evolution of cumulative reward over training episodes, while Figure 16 depicts the corresponding exploration ratio. The cumulative reward exhibits a nonlinear growth pattern, distinguishing it from the approximately linear trends observed in the tabular representation methods. Although the agent continues to accumulate rewards throughout training, the reduced growth rate suggests early convergence towards a sub-optimal policy, followed by limited performance improvement in later episodes. As shown in Figure 16, the

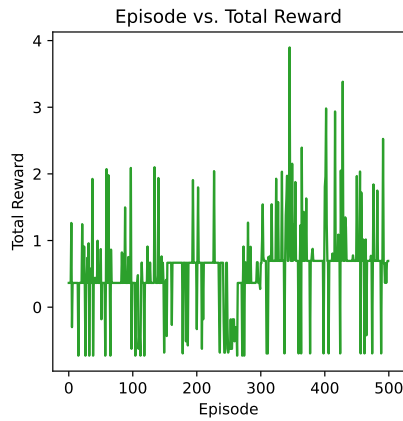


Figure 12. Episode versus total reward for the on-policy Q -learning agent with the function approximation method

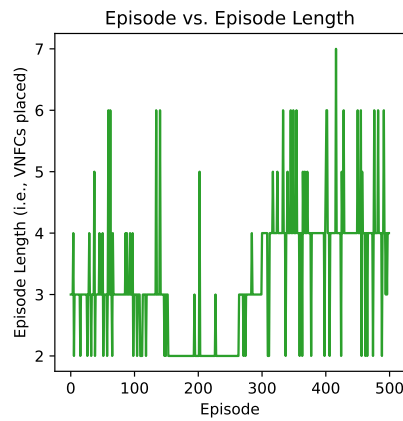


Figure 13. Episode versus episode length for the on-policy Q -learning agent with the function approximation method

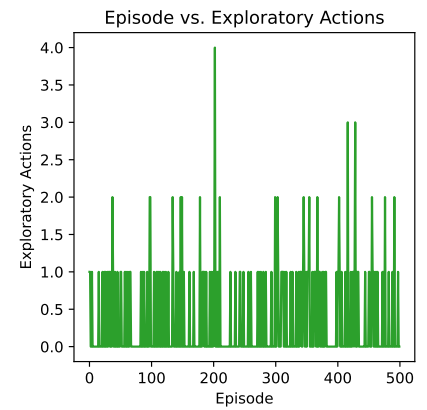


Figure 14. Episode versus exploratory actions for the on-policy Q -learning agent with the function approximation method

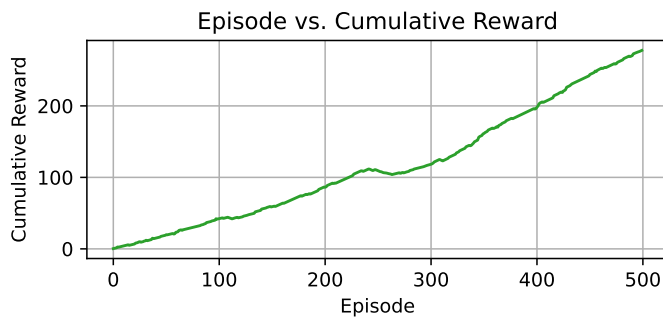


Figure 15. Episode versus cumulative reward for the on-policy Q -learning agent with the function approximation method

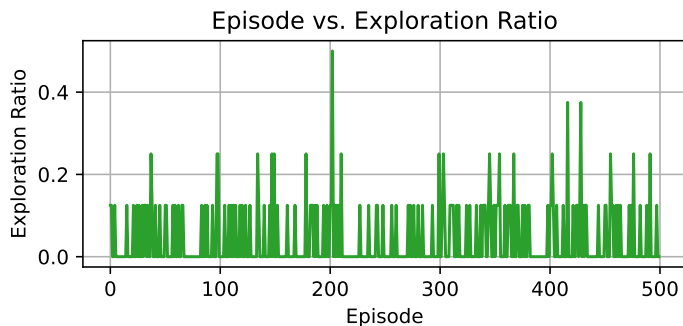


Figure 16. Episode versus exploration ratio for the on-policy Q -learning agent with the function approximation method

exploration ratio remains variable over the entire training horizon, with no evident decay trend. This behavior indicates that the fixed ϵ -greedy exploration strategy does not sufficiently reduce exploration as learning progresses. When combined with function approximation, this persistent exploration further constrains policy refinement, thereby contributing to premature convergence and limiting long-term performance gains.

Overall, the on-policy function approximation approach achieves comparatively efficient episode completion but exhibits inferior reward performance when compared to the tabular representation methods. These findings indicate that additional hyperparameter tuning—particularly with respect to the learning rate and exploration schedule—may be necessary to improve reward optimality, mitigate premature convergence,

and enhance overall policy stability.

4) *Off-Policy Function Approximation:* The learning behavior of the off-policy function approximation Q -learning agent over 500 episodes is illustrated in Figures 17–21.

Figure 17 illustrates the episode-wise total reward achieved by the off-policy Q -learning agent with function approximation. The reward signal exhibits noticeable stochastic fluctuations across episodes, with values ranging approximately from -1 to 3.5 and most episodes concentrated toward the lower end of the reward spectrum. In contrast to the tabular representations, and similarly to the on-policy function approximation case, the agent rarely attains near-optimal rewards under this configuration, indicating limited reward optimality. This behavior suggests that, despite the off-policy update mechanism, the learned policy does not fully stabilize across episodes when combined with function approximation. The approximation error introduced by the function estimator, together with the stochastic nature of the environment and continued exploratory behavior, contributes to the observed reward variability and sub-optimal performance.

Figures 18 and 19 provide further insights into the learning dynamics of the off-policy agent employing function approximation. As shown in Figure 18, the episode length predominantly varies between 2 and 7 steps, with a noticeable concentration toward shorter sequences. This trend indicates that the agent frequently completes the VNFC placement process efficiently, exhibiting execution behavior comparable to the on-policy function approximation approach. Figure 19 illustrates the number of exploratory actions per episode. The observed values generally remain low, typically ranging from 0 to 3, while following a stochastic pattern across training episodes. This behavior reflects the continued influence of the exploratory behavior policy in off-policy learning, resulting in persistent exploration that supports adaptability but also limits full exploitation of the learned action-value function.

Figures 20 and 21 present the evolution of cumulative reward and exploration ratio over training episodes, respectively. The cumulative reward increases in an approximately linear manner, confirming that the agent continues to accumulate rewards steadily over time. However, the relatively shallow slope of the cumulative reward curve suggests early conver-

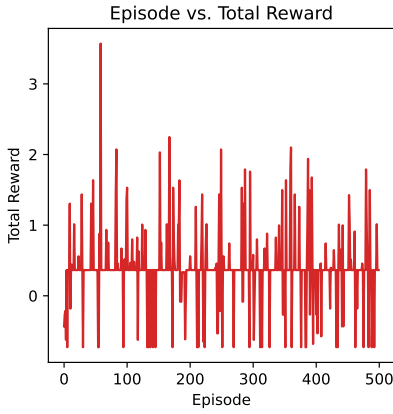


Figure 17. Episode versus total reward for the off-policy Q -learning agent with the function approximation method

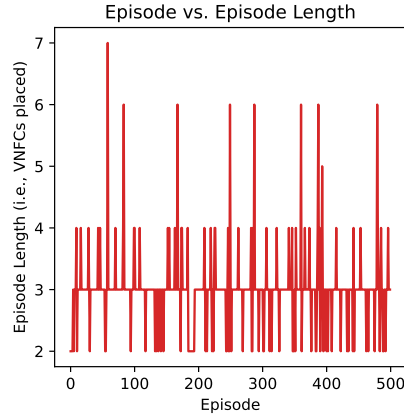


Figure 18. Episode versus episode length for the off-policy Q -learning agent with the function approximation method

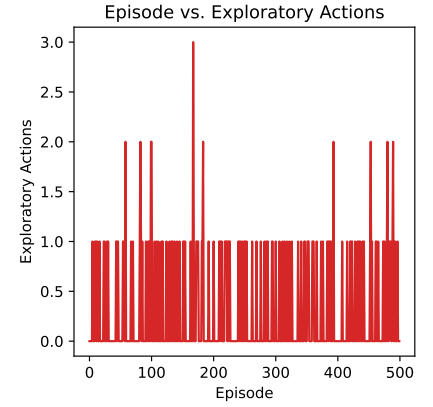


Figure 19. Episode versus exploratory actions for the off-policy Q -learning agent with the function approximation method

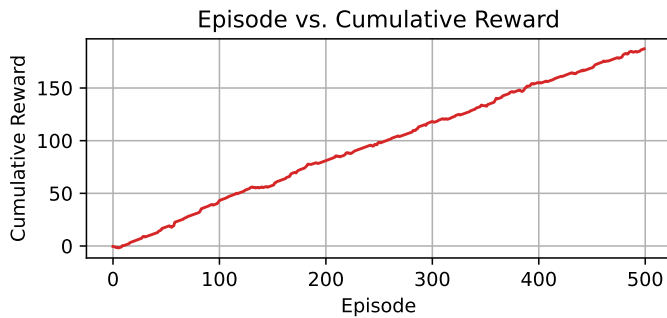


Figure 20. Episode versus cumulative reward for the off-policy Q -learning agent with the function approximation method

gence toward a suboptimal policy, with limited performance improvement observed in later training stages. As shown in Figure 21, the exploration ratio remains variable throughout the training process, with no evident decay trend. This behavior indicates that the fixed ϵ -greedy exploration strategy does not sufficiently reduce exploratory actions as learning progresses. When combined with function approximation, this persistent exploration further constrains policy refinement and contributes to the observed early convergence and limited long-term performance gains.

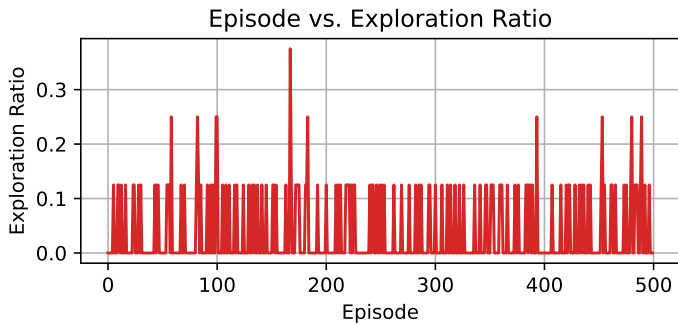


Figure 21. Episode versus exploration ratio for the off-policy Q -learning agent with the function approximation method

Overall, the off-policy function approximation approach exhibits the weakest performance among the four evaluated methods under the considered experimental settings. Although it achieves higher average rewards than its on-policy function approximation counterpart, this improvement comes at the

cost of increased variability, as reflected by a higher standard deviation. Furthermore, the method requires approximately 55 episodes to converge, which is the longest convergence duration observed among all four approaches. These results indicate that, despite the benefits of off-policy learning, the combination with function approximation leads to reduced stability and slower convergence in our study.

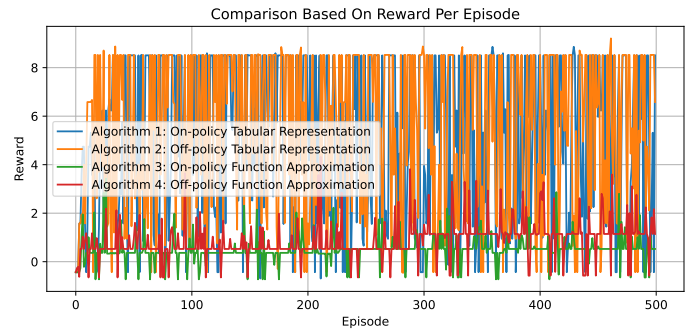


Figure 22. Comparison of reward per episode across the four Q -learning variants, illustrating the superior reward performance of tabular representation methods and the consistently lower reward levels achieved by function approximation approaches over the training horizon.

C. Comparative Results

In the considered experimental setting, a total of 100 VMs and 8 VNFCs are evaluated, resulting in a discrete VNFC-to-VM placement action space of $8 \times 100 = 800$ possible assignments. Under this configuration, the tabular representation methods consistently achieve higher per-episode rewards than the function approximation-based approaches. As reported in Table III, the off-policy tabular method attains the highest average reward of 5.42, whereas the on-policy function approximation method yields the lowest average reward of 0.50. Figure 22 illustrates the per-episode reward trajectories for all four methods, while Figure 23 presents the corresponding area-under-the-curve representation.

A similar performance trend is observed when comparing the reward per episode using the AUC metric in Figure 23. The off-policy tabular representation achieves the highest AUC value of 2705.03, followed by the on-policy tabular

Table III. Comparative evaluation of the four Q -learning variants in terms of average reward, reward variability, and convergence behavior.

Algorithm	Average Reward	Standard Deviation	Convergence Episode
Algorithm 1 (on-policy tabular representation)	5.12	3.35	15
Algorithm 2 (off-policy tabular representation)	5.42	3.23	13
Algorithm 3 (on-policy function approximation)	0.50	0.55	6
Algorithm 4 (off-policy function approximation)	0.89	0.76	55

method with an AUC of 2555.20. In contrast, the function approximation approaches exhibit substantially lower AUC values, with the on-policy function approximation achieving the lowest AUC of 248.75, and the off-policy function approximation reaching an AUC of 444.00. These results highlight the superior reward accumulation capability of tabular methods in the examined large discrete action space.

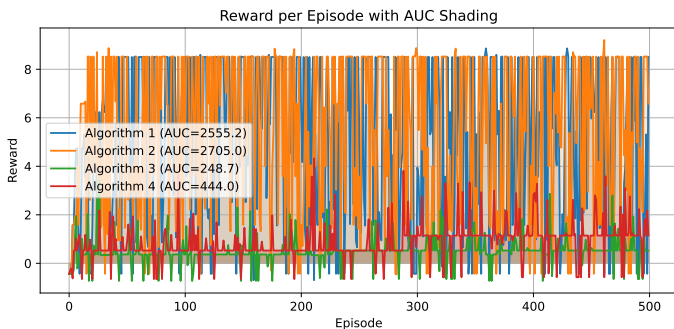


Figure 23. Comparison of reward per episode with AUC shading across the four Q -learning variants, highlighting the superior long-term reward accumulation of tabular representation methods and the substantially lower AUC achieved by function approximation approaches.

Although the tabular variants outperform their function approximation counterparts in terms of reward-based metrics under the considered setting, the function approximation approaches exhibit improved stability and faster convergence behavior. In particular, the on-policy function approximation method demonstrates lower standard deviation compared to the tabular methods, indicating more stable learning dynamics. With respect to convergence speed, the on-policy function approximation converges the fastest, requiring only 6 episodes, whereas the off-policy function approximation converges the slowest, taking 55 episodes to reach convergence.

Overall, the comparative analysis reveals a clear trade-off between reward optimality and learning stability across the evaluated Q -learning variants. While tabular representation methods consistently achieve superior reward accumulation in the considered large discrete action space, function approximation approaches offer faster convergence and improved stability at the cost of reduced reward performance.

VI. CONCLUDING REMARKS AND FUTURE OUTLOOK

In this paper, our goal was to address the VNFC-to-VM mapping problem within O-RAN by employing Q -learning. We implemented four distinct variants of Q -learning: two based on tabular representations (on-policy and off-policy tabular methods) and two based on function approximation (on-policy and off-policy function approximation methods). Upon successful implementation, we compared the performance of all four variants using a set of evaluation metrics.

The obtained results correspond to a specific VNFCs and VMs configuration; however, the observed trends are expected to generalize to other deployment scenarios. Given the specific dataset used in our experimental setting (comprising 8 VNFCs [representing the VNFCs of a complete O-RAN slice] and 100 VMs), we observed that tabular methods achieved higher average rewards per episode, in contrast to scenarios involving larger datasets. However, the on-policy function approximation method outperformed its counterparts in terms of convergence speed and exhibited greater stability, as indicated by a lower standard deviation. Therefore, depending on the optimization objective, the choice of method may vary. For instance, tabular methods may be preferred when maximizing reward, whereas the on-policy function approximation method may be more suitable when convergence speed and stability are prioritized. Ultimately, the well-known principle in ML, commonly referred to as the “no free lunch” phrase, applies.

In future work, we aim to extend the current research from both a methodological perspective (i.e., by exploring more advanced RL algorithms) and an applied perspective (i.e., applying the proposed approaches to practical use cases). First, we plan to implement deep Q -learning and double deep Q -learning algorithms to enhance the mapping of O-CU and O-DU, leveraging their ability to handle high-dimensional state spaces and improve convergence. Second, we intend to deploy these approaches in practical use cases, such as optimizing resource management, latency, energy consumption, and other key performance indicators (KPIs) in real-world scenarios. These efforts will further bridge the gap between theoretical frameworks and practical applications, enabling more efficient and adaptive solutions for O-RANs.

APPENDIX A

REVIEW OF EXISTING STATE-OF-THE-ART APPROACHES TO THE MAPPING PROBLEM

The VNF mapping problem has been extensively investigated in both cloud/data center networks and wireless networks using a wide range of methodological approaches. This appendix surveys the most recent and relevant contributions in the literature, with particular emphasis on the key challenges addressed by existing solutions. A structured overview of selected works is presented in Table IV, which compares the studies in terms of their objectives, employed methodologies, and the KPIs they optimize.

For clarity and systematic presentation, the reviewed literature is categorized into two groups: (i) approaches proposed for VNF mapping in cellular networks and (ii) approaches developed for cloud/data center networks. The table consolidates the analyzed works by summarizing their objectives,

Table IV. Summary of recent studies on VNF mapping, comparing objectives, methodologies, and KPIs in cellular and cloud/data center networks.

Category	Reference	Year	Objectives	KPIs	Methodology
Proposed approaches for VNF mapping in cloud/data center networks	Beloglazov <i>et al.</i> [12]	2013	Optimize VM consolidation, minimize energy consumption	Energy consumption and VM migrations	Markov chain model
	Xiao <i>et al.</i> [13]	2013	Prevent overload of PMs by effective VM placement to support green computing	No. of overloaded servers, No. of actively used PMs, No. of VM migrations, and energy savings	Fast up and slow down algorithm prediction
	Alameddine <i>et al.</i> [14]	2017	Optimize traffic routing and scheduling	Schedule length and execution time	Column generation with primal-dual decomposition
	Nejad <i>et al.</i> [15]	2018	Optimize VNF placement and admission control	Acceptance rate and revenue from VNF requests	Mixed integer linear programming
	Quang <i>et al.</i> [16]	2019	Optimize VNF placement	Acceptance ratio, resource utilization, and quality of service (QoS)	Enhanced exploration deep deterministic policy gradient
	Pei <i>et al.</i> [17]	2020	Minimize cost and improve performance in VNF placement	Request reject rate, throughput delay, and VNF utilization	Double deep Q network
	Pham <i>et al.</i> [18]	2020	Minimize operational and traffic costs for VNF service chain placement	Operational energy consumption, network latency, bandwidth usage, and total cost	Markov approximation and matching theory
	Azizi <i>et al.</i> [19]	2021	Minimize power consumption and resource wastage	Active PMs, resource wastage, and power consumption	Greedy randomized algorithm
	Sallam <i>et al.</i> [20]	2021	Maximize processed network flows under realistic constraints	Processed flow volume, budget usage, and capacity utilization	Integer programming and submodular optimization algorithms
	Kuai <i>et al.</i> [21]	2022	Maximize fairness in VNF mapping and scheduling across service function chains satisfying delay requirements	Minimum earliness and acceptance ratio	Proximal policy optimization and deep RL
	Seyyedsalehi <i>et al.</i> [10]	2022	Optimize VM placement in multi-data center clouds for big data tasks	Energy consumption, intra-data center traffic, VM migration, and service level agreement violations	Aware genetic algorithm first fit (AGAFF) algorithm
	Bagaa <i>et al.</i> [22]	2022	Optimize security orchestration considering QoS and heterogeneous resource constraints	End-to-end delay, bandwidth, resource utilization, and security levels	Linear programming and heuristic algorithms
Wei <i>et al.</i> [23]	2025	Adaptively map service function chains to minimize cost and network congestion	Service delay, bandwidth consumption, network load balancing, and acceptance ratio	Deep RL with long short-term memory	
Proposed approaches for VNF mapping	Mijumbi <i>et al.</i> [24]	2017	Predict VNF resource needs using topology-aware learning approaches	Predict accuracy, call drop rate, latency, and resource efficiency	Graph neural networks
	Domenico <i>et al.</i> [9]	2020	Optimize VNF deployment and resource allocation in hybrid cloud infrastructure	Resource usage, No. of supported slices, and latency complications	Integer linear programming
	Mei <i>et al.</i> [25]	2022	Optimize embedding of 5G slices with sharable VNFs to improve resource utilization	Slice acceptance ratio and physical resource utilization	Integer linear programming and heuristic algorithm
	Kist <i>et al.</i> [26]	2024	Enable RAN slicing with isolation, programmability, adaptability, and scalability	Slice isolation, performance, scalability and customization flexibility	Prototype combining baseband unit and remote radio head hypervisors
	Tran <i>et al.</i> [27]	2024	Optimize network throughput by maximizing the No. of service function chains embedded in the network	Acceptance ratio, network throughput ratio, and execution time	Deep-RL (specifically deep Q -learning and advantage actor critic approaches)
	Hojiej <i>et al.</i> [28]	2025	O-CU and O-DU placement in O-RAN	Maximizing user admittance, minimizing deployment costs, and increasing throughput	Recurrent neural network
Our paper	Habibi <i>et al.</i>	2026	Mapping the VNFCs of O-CU and O-DU within an O-RAN slice subnet onto O-Clouds in O-RAN	Minimize resource wastage while ensuring efficient and scalable VNFC mapping	RL (specifically the four variants of Q -Learning)

methodologies, and optimized KPIs, thereby highlighting both the diversity of proposed solutions and the specific VNF mapping challenges they address.

APPENDIX B

JUSTIFICATION FOR DECOMPOSING O-CU AND O-DU INTO VNFCs FOR ENHANCED O-RAN SLICING

We propose that decomposing O-CU and O-DU into VNFCs offers a promising approach for achieving fine-grained resource allocation, enhancing O-RAN slicing, and enabling more efficient mapping of O-CU and O-DU onto O-Cloud sites. This appendix outlines the advantages of this proposal, illustrating how splitting VNFs into VNFCs can improve operational flexibility, scalability, and fault tolerance while simultaneously optimizing the performance of O-RAN slices.

Enhanced O-RAN Slicing Flexibility: By decomposing O-CU and O-DU into VNFCs, each VNFC can be individually scaled and allocated to specific O-RAN slices based on their functional requirements or predefined policies. For instance, certain PDCP functionalities may introduce significant latency and therefore need to be disabled for O-RAN slices providing ultra-reliable low latency communications (URLLC) services. Similarly, some RLC functionalities, such as segmentation, might only be enabled for enhanced mobile broadband (eMBB) slices, while being disabled for URLLC and massive machine-type communications (mMTC) slices [8]. An additional benefit of this approach is that individual VNFCs can be instantiated, migrated, or modified without disrupting the entire O-CU or O-DU, enabling a more agile response to slice-specific needs in O-RAN.

Finer Control over Workload Distribution and Hardware Utilization: Splitting into VNFCs provides finer control

over workload distribution across different computing nodes or O-Cloud sites. For example, VNFCs requiring low latency can be deployed closer to the network edge, while those with less stringent latency demands may reside in centralized O-Cloud sites. Moreover, VNFC-level decomposition facilitates better utilization of heterogeneous hardware resources, such as graphics processing units (GPUs) for PHY-layer VNFCs or general central processing units (CPUs) for higher-layer VNFCs. Taken together, these benefits significantly optimize VNF mapping compared to traditional approaches.

Improved Fault Tolerance and Resilience: In this approach, if one VNFC experiences issues, the impact is limited to the specific functionality it provides. Hence, this isolation enhances the resilience and reliability of an O-gNB. Moreover, if a VNFC fails, it can be restarted or replaced without affecting other components within the O-CU or O-DU.

Facilitating Focused Optimization: With distinct VNFCs, AI/ML models can optimize specific functionalities more effectively. For example, predicting congestion for the PDCP VNFC or improving scheduling in the MAC VNFC. Moreover, granular monitoring of VNFCs generates more detailed metrics, which can be collected and utilized by AI/ML models to enhance performance analysis of the O-CU and O-DU.

Alignment with Microservice Architectures: Our proposal is aligned with microservice-based architectural principles, which emphasize modularity and ease of management. We believe that a VNFC-based architecture is more open to integrating functionalities, algorithms, and features from multiple vendors, adhering to the spirit of openness in O-RAN. For example, within the O-CU, an operator may select three VNFCs from different vendors, choosing each one based on its

Box 1. Proof: Equivalence Between the Expectation-Based Bellman Optimality Equation and the Q-Value Update Rule in Algorithm 1 and Algorithm 2

We begin with the Q-learning update rule (Equation [23]):

$$Q_{t+1}(S_t, A_t) = Q_t(S_t, A_t) - \alpha_t \left[Q_t(S_t, A_t) - \left(R_{t+1} + \gamma \max_{a \in \mathcal{A}(S_{t+1})} Q_t(S_{t+1}, a) \right) \right].$$

Rearranging the terms, we obtain:

$$Q_{t+1}(S_t, A_t) = (1 - \alpha_t)Q_t(S_t, A_t) + \alpha_t \left(R_{t+1} + \gamma \max_{a \in \mathcal{A}(S_{t+1})} Q_t(S_{t+1}, a) \right).$$

Since we are dealing with stochastic learning, the next reward, R_{t+1} , and the next state, S_{t+1} , are treated as random variables. Taking the expectation on both sides (conditioned on the current state-action pair $(S_t, A_t) = (s, a)$), we have:

$$\mathbb{E}[Q_{t+1}(S_t, A_t)|s, a] = \mathbb{E} \left[(1 - \alpha_t)Q_t(S_t, A_t) + \alpha_t \left(R_{t+1} + \gamma \max_{a \in \mathcal{A}(S_{t+1})} Q_t(S_{t+1}, a) \right) \middle| s, a \right].$$

$$\mathbb{E}[Q_{t+1}(s, a)] = (1 - \alpha_t)Q_t(s, a) + \alpha_t \mathbb{E} \left[R_{t+1} + \gamma \max_{a \in \mathcal{A}(S_{t+1})} Q_t(S_{t+1}, a) \middle| s, a \right],$$

where we use the linearity of expectation and the fact that $Q_t(s, a)$ is deterministic given (s, a) . At convergence, $Q_{t+1}(s, a) = Q_t(s, a) = Q^*(s, a)$, and the learning rate α_t cancels out, leaving:

$$Q^*(s, a) = \mathbb{E} \left[R_{t+1} + \gamma \max_{a \in \mathcal{A}(S_{t+1})} Q^*(S_{t+1}, a) \middle| S_t = s, A_t = a \right].$$

This corresponds to the Bellman optimality equation for Q^* (Equation [22]), thus establishing the equivalence. ■

superior performance compared to competing VNFCs in the market. This approach promotes innovation and competition.

Despite these advantages, decomposing the O-CU and O-DU into VNFCs presents several challenges that must be addressed to fully realize its potential, as discussed below.

Increased Overhead: Managing multiple VNFCs may introduce additional overhead in signaling, orchestration, and management of a VNF. Each VNFC requires its own control and monitoring mechanisms, increasing intercomponent communication for tasks such as state synchronization, fault detection, and load balancing. To mitigate this overhead, efficient lifecycle management strategies are needed, such as selectively instantiating specific VNFCs only when required and leveraging lightweight virtualization technologies (e.g., containers) to reduce the operational footprint.

Complexity: Decomposing the O-CU and O-DU can introduce complexity at multiple levels. First, managing a larger number of VNFC instances places additional demands on orchestration and automation frameworks (e.g., NFV-MANO), which must dynamically schedule and maintain these microservices across distributed O-Cloud sites. Second, cross-layer dependencies become more challenging, as individual VNFCs may require frequent state synchronization, resource sharing, or common security policies. Finally, this approach can complicate debugging, since identifying the root cause of performance issues or outages often involves tracing interactions across numerous microservices. Addressing these complexities necessitates robust management and orchestration solutions at the VNFC, VNF, and O-gNB levels.

APPENDIX C

EVALUATING THE SEQUENTIAL DECISION-MAKING NATURE OF MAPPING O-CU AND O-DU ONTO O-CLOUDS

The problem we address in this article, mapping a given VNFC onto a VM, is fundamentally a sequential decision-making optimization problem. This means that, rather than making all decisions simultaneously, the process unfolds iteratively, with one decision made at a given time. Each choice influences the subsequent decisions due to resource availability changes, dependencies between the VNFs, and the state of the underlying O-Clouds. This approach makes the sequence of actions critical to achieving optimal outcomes.

At each step of the mapping process, the task is to assign a VNFC to a suitable VM. For example, VNFC f_1 may be assigned to VM v_j based on current resource availability and placement constraints. Once this assignment is made, VM v_j becomes unavailable for subsequent allocations, as a one-to-one mapping is enforced. The process then proceeds iteratively to the assignment of VNFC f_i , for $i \in 2, \dots, 8$, in an environment that has now changed – some VMs, such as v_j in this example, are no longer available.

The process continues with each VNFC – from f_2 to f_8 – being placed one at a time, with the system state updating after each decision. Naturally, earlier allocation decisions constrain the options available for future assignments. For example, assigning a large VNFC to a VM with limited capacity early in the process may hinder the efficient placement of subsequent components, particularly if the remaining VMs lack sufficient resources to host the remaining VNFCs. This direct dependency, where earlier decisions influence the feasibility and quality of future ones, is a defining characteristic of a sequential decision-making problem.

Box 2. Proof: Equivalence Between the Expectation-Based Bellman Optimality Equation and the Q -Value Update Rule in Algorithm 3 and Algorithm 4

We start with the function approximation Q -update rule (Equation [28]):

$$Q_{t+1}(S_t, A_t) = Q_t + \alpha_t \left[R_{t+1} + \gamma \max_{a \in A(S_{t+1})} \hat{Q}(S_{t+1}, a, Q_t) - \hat{Q}(S_t, A_t, Q_t) \right] \nabla_Q \hat{Q}(S_t, A_t, Q_t).$$

Rearranging terms yields:

$$Q_{t+1}(S_t, A_t) = \left[Q_t - \alpha_t \hat{Q}(S_t, A_t, Q_t) \nabla_Q \hat{Q}(S_t, A_t, Q_t) \right] + \alpha_t \left[R_{t+1} + \gamma \max_{a \in A(S_{t+1})} \hat{Q}(S_{t+1}, a, Q_t) \right] \nabla_Q \hat{Q}(S_t, A_t, Q_t).$$

Let us define the term in the first square bracket as:

$$\beta := \left[Q_t - \alpha_t \hat{Q}(S_t, A_t, Q_t) \nabla_Q \hat{Q}(S_t, A_t, Q_t) \right].$$

Here, β captures deterministic terms. Since we are dealing with stochastic learning, the R_{t+1} and S_{t+1} are the random variables of significance. Hence, the other terms become insignificant. By taking the expectation (conditioned on $(S_t, A_t) = (s, a)$) on both sides of the aforementioned rearranged equation, we get:

$$\mathbb{E}[Q_{t+1}(S_t, A_t) | s, a] = \mathbb{E} \left[\beta + \alpha_t \left(R_{t+1} + \gamma \max_{a \in A(S_{t+1})} \hat{Q}(S_{t+1}, a, Q_t) \nabla_Q \hat{Q}(S_t, A_t, Q_t) \right) \middle| s, a \right].$$

$$\mathbb{E}[Q_{t+1}(s, a)] = \beta + \alpha_t \nabla_Q \hat{Q}(s, a, Q_t) \cdot \mathbb{E} \left[R_{t+1} + \gamma \max_{a \in A(S_{t+1})} \hat{Q}(S_{t+1}, a, Q_t) \middle| s, a \right].$$

The second equality follows from the linearity of the expectation operator \mathbb{E} . At convergence, $Q_{t+1} = Q_t = Q^*$, and α_t cancels out. Thus, the Bellman optimality equation emerges:

$$Q^*(s, a) = \mathbb{E} \left[R_{t+1} + \gamma \max_{a \in A(S_{t+1})} \hat{Q}(S_{t+1}, a, Q^*) \middle| S_t = s, A_t = a \right].$$

This matches the Equation (29), completing the proof. ■

Therefore, the VNFC-to-VM placement problem is inherently a sequential decision-making problem. This nature allows us to apply RL techniques, such as Q -learning – specifically through Algorithm 1, Algorithm 2, Algorithm 3, and Algorithm 4 – to learn a policy that selects actions (i.e., placements) in a manner that optimizes overall performance, such as minimizing resource wastage.

APPENDIX D

THE MATHEMATICAL DESCRIPTION OF THE VM PLACEMENT ONTO THE PM IN AN O-CLOUD SITE

Defining the virtual compute and storage workloads of VM(s) are vital metrics in the efficient placement of the VMs and the partitioning of the physical compute and storage resource of a PM, which is defined as follows [29]:

$$W_j = \frac{1}{1 - C_j^{max}} \times \frac{1}{1 - S_j^{max}}, \quad (30)$$

where the W_j is the total workload, C_j^{max} is the virtual compute demand, and S_j^{max} is the virtual storage demand of VM, $v_j \in \mathcal{V}$. It is worth noting that the virtual compute and storage workloads of a VM must not exceed (or overload) over 100%. Hence, the $C_j^{max} < W_j$ and the $S_j^{max} < W_j$. Based on Equation (30), the workloads of the O-CU and O-DU of an O-RAN slice on O-Cloud #1 and O-Cloud #2 are defined as follows:

$$W_{RAN} = 3 \cdot (W_j)_{j=1, \dots, 3} + 5 \cdot (W_j)_{j=4, \dots, 8}. \quad (31)$$

Likewise, defining the workloads of the PM(s), after placing the VM(s), is also a vital metric for optimal resource allocation and efficient management of physical resources of an O-Cloud, which is defined as follows [29]:

$$W_k = \frac{1}{1 - \left(C_k^{max} + \sum_{j=1}^m C_j^{max} \right)} \times \frac{1}{1 - \left(S_k^{max} + \sum_{j=1}^m S_j^{max} \right)} \quad (32)$$

, where W_k is the total workload, C_k^{max} is the current state of the compute resource workload, and S_k^{max} is the current state of the storage resource workload of PM, $p_k \in \mathcal{P}$.

The $\sum_{j=1}^m C_j^{max}$ is the total compute resource utilization and $\sum_{j=1}^m S_j^{max}$ is the total storage resource utilization of m VMs hosted by $p_k \in \mathcal{P}$. Do note that the total compute resource load and storage resource load of PM, p_k must not exceed (or overload) over 100%. Hence, the $C_k^{max} + \sum_{j=1}^m C_j^{max} < W_k$

and $S_k^{max} + \sum_{j=1}^m S_j^{max} < W_k$.

Defining the workloads of $v_j \in \mathcal{V}$ before placing onto $p_k \in \mathcal{P}$ is also vital to avoid the resource wastage of a PM and an O-Cloud. To achieve that goal, we define the compute and storage resource wastage of PM $p_k \in \mathcal{P}$ as follows [30]:

$$\psi_k = w_1 \times \frac{C_k^{ava}}{C_k^{cap}} + w_2 \times \frac{S_k^{ava}}{S_k^{cap}}, \quad (33)$$

such that w_1 and w_2 are weighting coefficients, C_k^{ava} are the available compute resources, and S_k^{ava} are the available

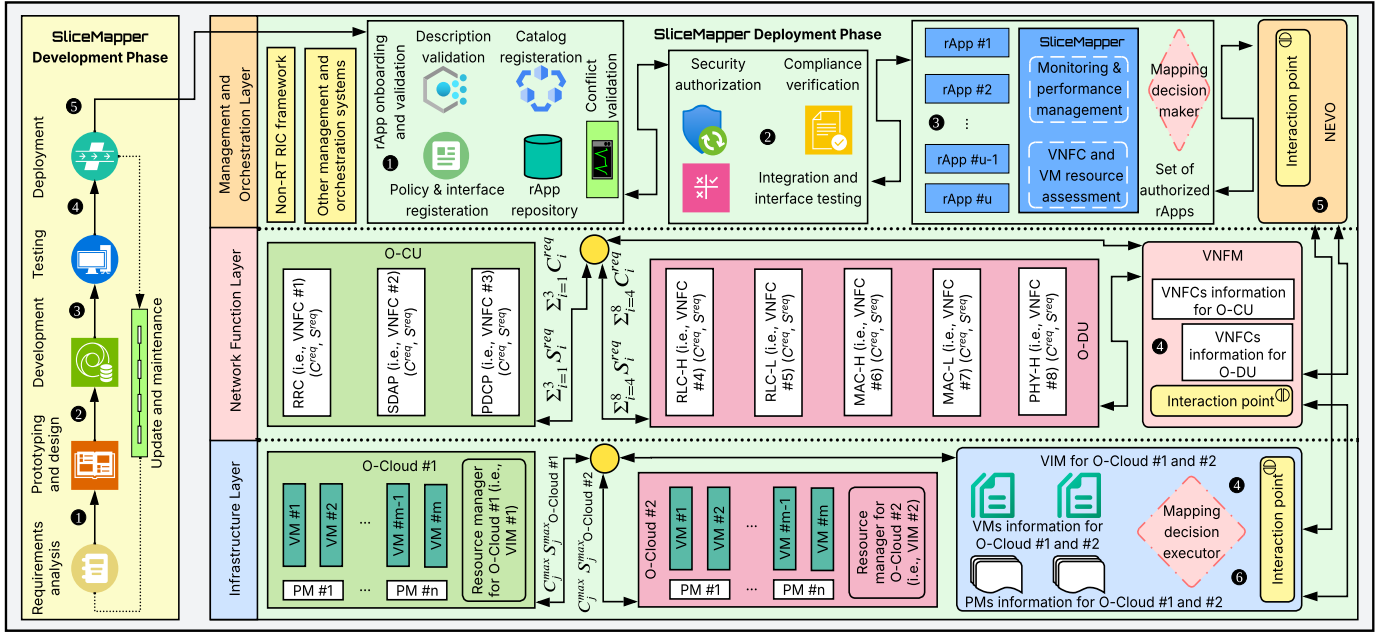


Figure 24. End-to-end standard-compliant development and deployment workflow of the SliceMapper for integration within O-RAN

storage resources on $p_k \in \mathcal{P}$ after the requested resources are assigned to its respective VMs, and C_k^{cap} is the compute resource capacity and S_k^{cap} is the storage resource capacity of the $p_k \in \mathcal{P}$. Likewise, the virtual compute and storage resource wastage of VM $v_j \in \mathcal{V}$ while taking ψ_k into account is calculated using the following equation [30]:

$$\zeta_j = w_1 \times \frac{C_j^{ava}}{C_j^{cap}} + w_2 \times \frac{S_j^{ava}}{S_j^{cap}} + \psi_k \cdot j, \quad (34)$$

such that C_j^{ava} are the available virtual compute resources and S_j^{ava} are the available virtual storage resources after $v_j \in \mathcal{V}$ hosts its respective VNFC, $f_i \in \mathcal{F}$, and C_j^{cap} is the virtual compute resource capacity and S_j^{cap} is the virtual storage resource capacity of the $v_j \in \mathcal{V}$.

APPENDIX E

PROOF OF CONVERGENCE TOWARDS THE BELLMAN OPTIMALITY EQUATION UNDER TABULAR REPRESENTATION METHOD

In this appendix, we prove the equivalence between the expectation-based Bellman optimality equation (22) and the Q -value updation rule (Equation [23]) employed in Algorithm 1 and Algorithm 2. The step-by-step derivation is detailed in Box 1. The proof begins with the tabular Q -update equation, highlighting how it can be algebraically rearranged to expose its dependency on the expected reward and maximum future Q -value. By taking the expectation over the stochastic reward and next state transitions, we derive an expression that aligns exactly with the Bellman optimality equation. This alignment confirms that the Q -learning updates in both algorithms, under convergence, lead to the optimal action-value function $Q^*(s, a)$. Consequently, this justifies the theoretical soundness of both Algorithm 1 and Algorithm 2 in approximating optimal decision-making policies for tasks performed by SliceMapper.

APPENDIX F

PROOF OF CONVERGENCE TOWARDS THE BELLMAN OPTIMALITY EQUATION UNDER FUNCTION APPROXIMATION METHOD

In this appendix, we prove the equivalence between the expectation-based Bellman optimality equation (Equation [29]) and the Q -value updation rule (Equation [28]) used in Algorithm 3 and Algorithm 4, both of which utilize function approximation method. The step-by-step derivation is presented in Box 2. Beginning with the Q -updation rule using a differentiable function approximator \hat{Q} , we algebraically restructure the equation to isolate stochastic components (rewards and state transitions). By introducing an intermediate term β for clarity and taking expectations, we demonstrate that the expression reduces to the Bellman optimality condition generalized for function approximation. This result confirms that the update rules in Algorithm 3 and Algorithm 4 converge to an optimal value function Q^* , thereby theoretically justifying their use in SliceMapper's learning framework.

APPENDIX G

STANDARD-COMPLIANT DEVELOPMENT AND DEPLOYMENT WORKFLOW OF SLICEMAPPER

In this appendix, we present an end-to-end standard-compliant workflow for the real-world integration of SliceMapper within O-RAN. As shown in Figure 24, the proposed workflow is structured into the Development Phase and the Deployment Phase. Each phase is described as follows.

Development Phase: This phase comprises several processes, as illustrated on the left-hand side of Figure 24. Each process ensures that SliceMapper is functionally correct, architecturally aligned with O-RAN principles, and technically prepared for operational integration within the SMO.

The Development Phase begins with a requirements analysis stage, during which the functional and non-functional objectives of the SliceMapper are formally specified. Based

on these requirements, a high-level architectural design of the *SliceMapper* is derived. The interaction model with the SMO (specifically the Non-RT RIC) is then formally defined, including the relevant service interfaces and data exchange mechanisms. Where appropriate, an initial prototype is implemented to validate feasibility, verify algorithmic assumptions, and ensure compatibility with the expected service interfaces prior to full-scale implementation. At this stage, the *SliceMapper* is packaged as container images and is considered ready for deployment preparation.

Prior to deployment, a comprehensive set of tests is conducted to ensure the correctness, stability, and interoperability of the rApp, particularly with respect to the VNFC-to-VM mapping functionality. Upon successful validation, the *SliceMapper* is prepared for transition to the Deployment Phase. The final onboarding artifacts – including the rApp descriptor, container image references, configuration files, and technical documentation – are consolidated into a release bundle. At this point, the *SliceMapper* is deemed deployment-ready and can proceed to formal onboarding, authorization, and infrastructure-level validation within the SMO.

Finally, this phase also includes the update and maintenance stage to enable the long-term reliability, security, and performance of the *SliceMapper* following its initial release. This stage includes periodic *SliceMapper* updates, security patching, performance optimization, and compatibility adjustments to accommodate evolving O-RAN specifications or infrastructure changes. In this stage, continuous improvement mechanisms are applied to address detected issues, incorporate feature enhancements, and maintain operational stability of *SliceMapper* across successive releases.

Deployment Phase: This phase is executed across all three layers proposed in the system model (see Section II), as illustrated on the right-hand side of Figure 24. It commences with the onboarding and system-level validation stage. First, the rApp descriptor undergoes description validation to ensure that metadata definitions, declared interfaces, and resource requirements align with the specifications of the SMO. Subsequently, policy and interface registration is performed. This stage guarantees that the rApp’s intended interactions are recognized and properly integrated within the Non-RT RIC. Following interface validation, the rApp is recorded in the system catalog through a catalog registration process. The validated package is then stored in the designated rApp repository. In addition, a conflict validation procedure is conducted to detect potential operational inconsistencies.

Following this, the rApp proceeds to the security authorization and operational testing stage. In this stage, the rApp undergoes a security assessment to ensure that it complies with the security policies of O-RAN. Compliance verification is subsequently performed to confirm adherence to regulatory requirements, operator-specific policies, and data protection constraints. In parallel, integration and interface testing are conducted to validate correct interaction with registered service interfaces and management components. Successful completion of this stage results in formal authorization for deployment and runtime activation of *SliceMapper*. The *SliceMapper* is then added to the list of authorized and

activated rApps within the Non-RT RIC.

Subsequently, the *SliceMapper* performs infrastructure-level resource assessment and mapping decision-making to enable operational deployment. First, the C_i^{req} and S_i^{req} of the VNFCs associated with the O-CU and O-DU are collected through the NFV-MANO-defined interfaces from the virtual network function manager (VNFM). The VNFM collects this information directly from the two VNFs. In parallel, the available resource information and capacity profiles of the candidate VMs, i.e., C_j^{max} and S_j^{max} , are gathered from the VIM. The VIM obtains this information directly from the VIMs associated with the two O-Cloud sites.

Based on these two types of information, the *SliceMapper* conducts a comprehensive assessment of VNFC requirements and VM capacities to determine feasible and efficient placement options. Subsequently, a mapping decision is made to assign each VNFC to an appropriate VM in accordance with resource constraints and deployment policies, using different variants of Q -learning algorithms. The finalized mapping decision is then forwarded to the network function virtualization orchestrator (NFVO), which communicates the placement instruction through the internal NFV-MANO interface to the VIM for execution. Upon successful execution, the VNFC-to-VM mapping is instantiated within the infrastructure, thereby preparing the *SliceMapper* for operational activation. Finally, the rApp continuously monitors the performance of the deployed mapping and dynamically adapts the placement if performance degradation or resource imbalance is detected.

ACKNOWLEDGMENT

This research was partially supported by the German Federal Ministry of Research, Technology and Space (BMFTR) through the Open6GHub+ project (Grant No. 16KIS2402K) and 6G Terafactory project (Grant No. 16KISK186). The authors gratefully acknowledge the anonymous reviewers for their insightful comments and constructive feedback, which significantly improved the quality of this article. The authors also thank the Area Editor and the Associate Editor for their efforts in coordinating the peer-review process.

ACRONYM LIST

5G fifth-generation
6G sixth-generation
AI artificial intelligence
AUC area under the curve
CPU central processing unit
eMBB enhanced mobile broadband
ETSI European Telecommunications Standards Institute
GPU graphics processing unit
KPI key performance indicator
MAC medium access control
ML machine learning
mMTC massive machine-type communications
NFV-MANO network function virtualization-management and orchestration
NFVO network function virtualization orchestrator
Non-RT RIC non-real-time RAN intelligent controller

NP nondeterministic polynomial time
O-Cloud open-cloud
O-CU open centralized unit
O-DU open distributed unit
O-gNB open next generation node B
O-RAN open radio access network
O-RU open radio unit
PDCP packet data convergence protocol
PHY physical
PM physical machine
QoS quality of service
RLC radio link control
RL reinforcement learning
RRC radio resource control
SARSA state action reward state action
SDAP service data adaptation protocol
SMO service management and orchestration
URLLC ultra-reliable low latency communications
VIM virtualized infrastructure manager
VM virtual machine
VNF virtual network function
VNFC virtual network function component
VNFM virtual network function manager

REFERENCES

- [1] W. Attaoui *et al.*, "VNF and CNF placement in 5G: Recent advances and future trends," *IEEE Trans. Netw. Serv. Manag.*, vol. 20, no. 4, pp. 4698–4733, 2023.
- [2] H. Talebian *et al.*, "Optimizing virtual machine placement in IaaS data centers: Taxonomy, review and open issues," *Cluster Computing*, vol. 23, p. 837–878, 2020.
- [3] M. A. Habibi, F. Z. Yousaf, and H. D. Schotten, "Mapping the VNFs and VLs of a RAN slice onto intelligent PoPs in beyond 5G mobile networks," *IEEE Open J. Commun. Soc.*, vol. 3, pp. 670–704, 2022.
- [4] K. Alam *et al.*, "A comprehensive tutorial and survey of O-RAN: Exploring slicing-aware architecture, deployment options, use cases, and challenges," *IEEE Commun. Surv. Tutor.*, vol. 28, pp. 1637–1678, 2026.
- [5] O-RAN Alliance, "Working Group 1; O-RAN Architecture Description; Technical Specification; V15.00." Alfter, Germany, Oct. 2025.
- [6] O-RAN Alliance, "Working Group 2; O-RAN Non-RT RIC Architecture; Technical Report; V07.00." Alfter, Germany, Jun. 2025.
- [7] M. A. Habibi *et al.*, "Unlocking O-RAN potential: How management data analytics enhances SMO capabilities?," *IEEE Open Journal of the Communications Society*, vol. 5, pp. 4710–4730, 2024.
- [8] O. Adamuz-Hinojosa *et al.*, "Sharing gNB components in RAN slicing: A perspective from 3GPP/NFV standards," in *IEEE Conference on Standards for Communications and Networking (CSCN)*, pp. 1–7, 2019.
- [9] A. De Domenico, Y.-F. Liu, and W. Yu, "Optimal virtual network function deployment for 5G network slicing in a hybrid cloud infrastructure," *IEEE Trans. Wirel. Commun.*, vol. 19, no. 12, pp. 7942–7956, 2020.
- [10] S. M. Seyedsalehi and M. Khansari, "Virtual machine placement optimization for big data applications in cloud computing," *IEEE Access*, vol. 10, pp. 96112–96127, 2022.
- [11] S. Zhao, *Mathematical Foundations of Reinforcement Learning*. New York, NY, USA: Springer, 2025.
- [12] A. Beloglazov and R. Buyya, "Managing overloaded hosts for dynamic consolidation of virtual machines in cloud data centers under quality of service constraints," *IEEE Trans. Parallel Distrib. Syst.*, vol. 24, no. 7, pp. 1366–1379, 2013.
- [13] Z. Xiao, W. Song, and Q. Chen, "Dynamic resource allocation using virtual machines for cloud computing environment," *IEEE Trans. Parallel Distrib. Syst.*, vol. 24, no. 6, pp. 1107–1117, 2013.
- [14] H. A. Alameddine, S. Sebbah, and C. Assi, "On the interplay between network function mapping and scheduling in VNF-based networks: A column generation approach," *IEEE Trans. Netw. Serv. Manag.*, vol. 14, no. 4, pp. 860–874, 2017.
- [15] M. A. T. Nejad *et al.*, "vSPACE: VNF simultaneous placement, admission control and embedding," *IEEE J. Sel. Area Commun.*, vol. 36, no. 3, pp. 542–557, 2018.
- [16] P. T. A. Quang, Y. Hadjadj-Aoul, and A. Outtagarts, "A deep reinforcement learning approach for VNF forwarding graph embedding," *IEEE Trans. Netw. Serv. Manag.*, vol. 16, no. 4, pp. 1318–1331, 2019.
- [17] J. Pei *et al.*, "Optimal VNF placement via deep reinforcement learning in SDN/NFV-enabled networks," *IEEE J. Sel. Area Commun.*, vol. 38, no. 2, pp. 263–278, 2020.
- [18] C. Pham *et al.*, "Traffic-aware and energy-efficient VNF placement for service chaining: Joint sampling and matching approach," *IEEE Trans. Netw. Serv. Manag.*, vol. 13, no. 1, pp. 172–185, 2020.
- [19] S. Azizi *et al.*, "GRVMP: A greedy randomized algorithm for virtual machine placement in cloud data centers," *IEEE Syst. J.*, vol. 15, no. 2, pp. 2571–2582, 2021.
- [20] G. Sallam and B. Ji, "Joint placement and allocation of VNF nodes with budget and capacity constraints," *IEEE/ACM Trans. Netw.*, vol. 29, no. 3, pp. 1238–1251, 2021.
- [21] Z. Kuai, T. Wang, and S. Wang, "Fair virtual network function mapping and scheduling using proximal policy optimization," *IEEE Trans. Commun.*, vol. 70, pp. 7434–7445, 2022.
- [22] M. Bagaa *et al.*, "QoS and resource-aware security orchestration and life cycle management," *IEEE Trans. Mob. Comput.*, vol. 21, no. 8, pp. 2978–2993, 2022.
- [23] W. Wei *et al.*, "An adaptive service function chains mapping with multi-task deep reinforcement learning," *IEEE Trans. Network Sci. Eng.*, vol. 12, no. 4, pp. 3093–3107, 2025.
- [24] R. Mijumbi *et al.*, "Topology-aware prediction of virtual network function resource requirements," *IEEE Trans. Netw. Serv. Manag.*, vol. 14, no. 1, pp. 106–120, 2017.
- [25] C. Mei *et al.*, "5G network slices embedding with sharable virtual network functions," *J. Commun. Net.*, vol. 22, no. 5, pp. 415–427, 2020.
- [26] M. Kist *et al.*, "Airtime: End-to-end virtualization layer for ran-as-a-service in future multi-service mobile networks," *IEEE Trans. Mob. Comput.*, vol. 21, no. 8, pp. 2701–2717, 2022.
- [27] T. D. Tran *et al.*, "5G service function chain provisioning: A deep reinforcement learning-based framework," *IEEE Trans. Netw. Serv. Manag.*, vol. 21, no. 6, 2024.
- [28] H. Hojeij *et al.*, "On flexible placement of O-CU and O-DU functionalities in Open-RAN architecture," *IEEE Trans. Netw. Serv. Manag.*, vol. 22, no. 1, pp. 660–674, 2025.
- [29] T. Wood *et al.*, "Sandpiper: Black-box and gray-box resource management for virtual machines," *Comput. Net.*, vol. 53, no. 17, pp. 2923–2938, 2009.
- [30] M. K. Hussein, M. H. Mousa, and M. A. Alqarni, "A placement architecture for a container as a service (CaaS) in a cloud environment," *J. of Cloud Comput.*, vol. 8, no. 7, p. 1–15, 2019.

AUTHOR BIOGRAPHIES



MOHAMMAD ASIF HABIBI received the B.Sc. degree in Telecommunication Engineering from Kabul University, Afghanistan, in 2011, the M.Sc. degree in Systems Engineering and Informatics from the Czech University of Life Sciences, Czech Republic, in 2016, and the Dr.-Ing. degree (Summa Cum Laude) from the University of Kaiserslautern (RPTU), Germany, in 2025. From 2011 to 2014, he worked as a Radio Access Network Engineer at Huawei. From 2017 to 2025, he was a Researcher and Senior Researcher with the Division of Wireless Communications and Radio Navigation, University of Kaiserslautern (RPTU), Germany. Since 2026, he has been a Senior Researcher at the German Research Center for Artificial Intelligence (DFKI). His research interests include network and service management, network architecture, machine learning, and radio access networks.



XAVIER COSTA-PÉREZ (M'06–SM'18) is Head of 6G Networks R&D at NEC Laboratories Europe, Scientific Director at the i2Cat R&D Center, and Research Professor at ICREA. His team contributes to products roadmap evolution as well as to European Commission R&D projects and received several awards for successful technology transfers. In addition, the team contributes to related standardization bodies: 3GPP, ETSI NFV, ETSI MEC, and IETF. Xavier has been a 5GPPP Technology Board member, served on the Program Committee of several conferences (including IEEE Greencom, WCNC, and INFOCOM), published at top research venues, and holds several patents. He also serves as Editor of IEEE Transactions on Mobile Computing and Transactions on Communications journals. He received both his M.Sc. and Ph.D. degrees in Telecommunications from the Polytechnic University of Catalonia (UPC) in Barcelona and was the recipient of a national award for his Ph.D. thesis.



HANS D. SCHOTTEN (S'93–M'97) received the Diploma and Ph.D. degrees in electrical engineering from the Aachen University of Technology, Germany, in 1990 and 1997, respectively. Since August 2007, he has been a full professor and head of the Division of Wireless Communications and Radio Navigation at University of Kaiserslautern (RPTU). Since 2012, he has also been Scientific Director at the German Research Center for Artificial Intelligence, heading the Intelligent Networks department. He was a senior researcher, the project manager, and the head of the research groups at Aachen University of Technology, Ericsson Corporate Research, and Qualcomm Corporate R&D. During his time at Qualcomm, he has also been the Director for Technical Standards and Coordinator of Qualcomm's activities in European research programs.